Acta Neuropathologica (2025) 149:51
https://doi.org/10.1007/s00401-025-02888-1

ORIGINAL PAPER

Annexin A6 membrane repair protein protects against amyloid-induced dystrophic neurites and tau phosphorylation in Alzheimer's disease model mice

Katherine R. Sadleir[1] · Karen P. Gomez[1] · Abigail E. Edwards[1] · Armana J. Patel[1] · Makenna L. Ley[1] · Ammaarah W. Khatri[1] · Joanna Guo[1] · Shreya Mahesh[1] · Elyse A. Watkins[1] · Jelena Popovic[1] · Devi Krishna Priya Karunakaran[1] · Dmitry Prokopenko[2] · Rudolph E. Tanzi[2] · Bernabe Bustos[1,3] · Steven J. Lubbe[1,3] · Alexis R. Demonbruen[4,5] · Elizabeth M. McNally[5] · Robert Vassar[1,6]

Received: 2 February 2025 / Revised: 23 April 2025 / Accepted: 30 April 2025

Abstract

In Alzheimer's disease, accumulation of amyloid-β (Aβ) peptide is thought to cause formation of neurofibrillary tangles composed of hyperphosphorylated tau protein, which correlates with neuronal loss and cognitive impairment, but the mechanism linking Aβ and tau pathologies is unknown. Dystrophic neurites, which surround Aβ plaques and accumulate phosphorylated tau and other proteins, may play a role in seeding and spreading of pathologic tau. Here, we investigate the novel hypothesis that improved membrane repair capacity decreases dystrophic neurite formation by protecting axons from Aβ-induced membrane damage. Using a ratiometric calcium sensor and a FRET-based calpain cleavage sensor, we demonstrate that dystrophic neurites in 5XFAD mice have elevated resting calcium levels and calpain activity because of putative membrane damage. Annexin A6, a plasma membrane repair in muscle and neurons, is present at plasma membrane of neurons and dystrophic neurites in murine and human brains. Overexpression of annexin A6 in brains of 5XFAD mice decreased size and quantity of dystrophic neurites and accumulation of phospho-tau181, an early biomarker of amyloid pathology. Phospho-tau231, another early amyloid biomarker, and phosphorylated of tau kinases, c-jun N-terminal kinase (JNK) and Calmodulin Kinase II (CaMKII) accumulate in dystrophic neurites in the brains of amyloid pathology mice and humans with AD, suggesting that dystrophic neurites are sites of active tau phosphorylation. Overexpression of dominant-negative annexin A6 in 5XFAD mice increased dystrophic neurites and phospho-tau181. Intracerebral injection of recombinant annexin A6 in 5XFAD and APP-NLGF knock-in mice resulted in localization of recombinant A6 to membranes of dystrophic neurites, suggesting therapeutic potential of recombinant annexin A6 for AD. In conclusion, dystrophic neurites have Aβ-induced membrane damage characterized by calcium elevation, calpain activation, and accumulation of tau kinases and phosphorylated tau. Overexpression of annexin A6 reduces dystrophic neurites and phospho-tau accumulation, suggesting that annexin A6-mediated membrane repair may represent a novel therapeutic approach for AD.

Keywords Amyloid pathology · Tau phosphorylation · Membrane repair · Alzheimer's disease · Calcium dysregulation · Dystrophic neurites

✉ Katherine R. Sadleir
krdoherty@northwestern.edu

✉ Robert Vassar
r-vassar@northwestern.edu

[1] Department of Neurology, Feinberg School of Medicine, Northwestern University, Chicago, IL 60611, USA

[2] Department of Neurology, Genetics and Aging Research Unit and the McCance Center for Brain Health, Massachusetts General Hospital and Harvard Medical School, Charlestown, MA, USA

[3] Simpson Querrey Center for Neurogenetics, Feinberg School of Medicine, Northwestern University, Chicago, IL, USA

[4] Department of Pharmacology, Feinberg School of Medicine, Northwestern University, Chicago, IL, USA

[5] Center for Genetic Medicine, Feinberg School of Medicine, Northwestern University, Chicago, IL, USA

[6] Mesulam Center for Cognitive Neurology and Alzheimer's Disease, Feinberg School of Medicine, Northwestern University, Chicago, IL, USA

Published online: 24 May 2025

Introduction

Alzheimer's disease (AD) is the most common cause of dementia affecting 6.7 million people in the US [1]. While therapeutic agents targeting AD pathologies, β-amyloid (Aβ) plaques and tau neurofibrillary tangles (NFTs), are in development and anti-Aβ monoclonal antibodies have been given FDA approval (*e.g.*, aducanumab [2], lecanemab, and donanemab) [84], there is still need to develop disease-modifying therapeutics targeting other pathologic mechanisms of AD to be used separately or in combination. Anti-Aβ antibodies slow but do not halt or reverse AD progression, while benefiting only early AD and having potentially serious side effects. Therefore, discovering novel disease-modifying drugs that can benefit all stages of AD with minimal adverse effects is a high priority in the field.

Accumulation of cerebral Aβ precedes the formation of tau tangles by at least 2 decades in AD [5, 18, 49, 50, 57–59, 69, 80, 87, 88]. Moreover, amyloid-positivity is associated with cognitive decline and tau accumulation [15, 49, 83, 87]. This evidence suggests that toxic Aβ species (*e.g.*, oligomers, protofibrils, and fibrils) trigger pathologic tau (tau hyperphosphorylation, fragmentation, and NFTs), which is associated with synapse and neuron loss (reviewed in [66] Although the mechanism linking Aβ and tau in AD is a profound mystery, disrupting the link between amyloid and tau pathologies, especially before cognitive impairment, may represent an effective therapeutic strategy for preventing AD.

Dystrophic neurites (DNs) are swollen neuronal processes, mostly axons [77, 98, 106], which form near amyloid plaques in the AD brain, often creating a halo that surrounds and is in contact with the plaque (reviewed in [111]). DNs accumulate proteins involved in AD, such as amyloid precursor protein (APP) [4, 22, 24, 62], β-site APP cleaving enzyme 1 (BACE1) [64, 98, 121], and abnormally phosphorylated tau (reviewed in [32]). We and others hypothesize that accumulation of phosphorylated, truncated, and aggregated tau in plaque-associated DNs plays a key role in the spread of pathologic tau throughout the brain [10, 53, 73, 119] and may link Aβ and tau pathologies. It has long been observed that DNs around cored plaques stain with antibodies to a variety of different pathological phospho-tau epitopes, such as AT8, and antibodies recognizing paired helical filaments (PHF) [32]. Increased cerebral spinal fluid (CSF) and plasma levels of tau phospho-isoforms, such as p-tau181, p-tau217, and p-tau231, accurately predict amyloid-positivity by positron emission tomography (PET) and are robust biomarkers of AD status and severity [19, 45, 60, 65, 107], further supporting a link between Aβ and tau. A direct relationship exists between the amount of neuritic dystrophy around Aβ plaques and the spread of pathologic tau from one hemisphere to the other in amyloid mouse models after injection of tau seeds isolated from human AD brain [47, 53, 72, 97]. Mouse models, such as 5XFAD, with many neuritic plaques have more extensive tau spreading than those with fewer or more diffuse plaques, such as APP-NLF knock-in mice [53]. Additionally, mutations in *TREM2* result in increased DNs around plaque and promote pathologic tau spreading in mouse models [72]. Moreover, humans with no cognitive impairment, but levels of amyloid plaques similar to those of AD patients at autopsy (termed asymptomatic AD), had significantly less phospho-tau accumulation around plaques, implicating DN-associated phospho-tau in cognitive decline [63]. Interestingly, tau isolated from these asymptomatic AD brains had aggregation states and seeding properties that were comparable to tau isolated from amyloid plaque-free control brains and lower than tau isolated from AD brains [63]. Together, these data suggest that preventing the formation of DNs should slow the development of tau pathology and benefit cognition.

Although an association exists between Aβ plaques and DNs, the mechanism of DN formation is unclear. One hypothesis is that DNs result from axonal membrane damage caused by contact with Aβ in plaques. Aβ peptides, especially longer isoforms, like 42 amino-acid Aβ42, are very hydrophobic and may injure cell membranes. Indeed, evidence suggests that neuronal membrane damage caused by Aβ could be involved in the etiology of AD [33, 37, 51]. One of the most direct effects of plasma membrane damage is increased intracellular calcium. The calcium hypothesis of AD posits that dysregulation of calcium homeostasis is the point of convergence of many risk factors and molecular mechanisms that lead to development of AD and its associated neurodegeneration [3, 67]. Basal intracellular calcium levels are abnormally elevated in neuronal soma and DNs near amyloid plaques in *APP* transgenic mice, such that an increasing calcium concentration gradient is observed approaching the plaque, as opposed to regions distant from plaques in which calcium levels appear normal [68]. Increased intracellular calcium can affect activity of tau kinases and phosphatases and activate calpain cleavage of tau [38, 91, 103], which can create toxic tau fragments [91] and affect tau phosphorylation and aggregation states (reviewed in [11]). Overexpression of the endogenous calpain inhibitor calpastatin and pharmacological inhibition of calpain have been shown to ameliorate the phenotypes of amyloid and tau mouse models [74, 82].

Since membrane damage is a common threat to cellular viability, mechanisms have evolved to repair and reseal the plasma membrane. This function is probably most important in tissues with long-lived cells that suffer mechanical

stress, such as skeletal and cardiac muscle, and have limited replacement potential, such as neurons [29]. The annexin family of proteins exhibit broad tissue distribution and function in membrane and actin remodeling, immune cell modulation, and wound repair [48]. Annexin A6 (A6) plays a key role in membrane resealing in skeletal muscle, heart, and neurons, and recombinant A6 shows therapeutic potential in these systems [30, 31]. Like other annexins, A6 binds negatively charged phospholipids, such as phosphatidylserine, phosphatidic acid, and phosphoinositides, in the presence of calcium [44]. Additionally, A6 is unique among the annexins in that the gene originated from a genomic duplication resulting in eight calcium-binding repeats rather than four (Fig. 3A). Upon acute membrane injury, A6 binds calcium and initiates the formation of a repair cap protein complex at the site of damage (Fig. 3B) [31]. After calcium binding, annexin A6 [34, 99, 116] then recruits other proteins in the repair complex, annexins A1 and A2 [34, 90], and the shoulder proteins BIN1 [40, 110], dysferlin [39, 54], and the EHD family proteins [12, 13, 43], which are all expressed in brain. *BIN1* is a strong GWAS AD risk factor [26, 27, 70, 102], suggesting that the membrane repair function of BIN1 may be compromised in AD. A truncation mutant resulting in only the N-terminal 32 amino acids of annexin A6, p.N32* [108], and a missense mutation that is deficient in calcium binding, p.E233 A [30], both exert a strong dominant-negative effect on repair cap assembly, supporting the key role of annexin A6 in membrane repair.

Recently, we have demonstrated that acute plasma membrane laser injury of annexin A6-GFP knock-in mouse primary neurons results in rapid recruitment of A6-GFP at the site of injury [29], similar to the well-established laser-induced muscle injury paradigm [28, 30, 31, 108]. In skeletal and heart muscle cells, exogenous recombinant annexin A6 (rA6) localizes rapidly to the site of laser injury and enhances membrane repair, suggesting that rA6 may offer a novel therapeutic approach [29, 30]. Similarly, we have shown that recombinant tdTomato-tagged annexin A6 added to the media colocalized with genomically expressed annexin A6-GFP at the site of laser injury site in both neuronal soma and neurites of primary neurons [29]. These results suggest that, like in muscle, either annexin A6 gene therapy or exogenous rA6 administration could be used therapeutically to mediate neuronal membrane repair in the brain. These *in vitro* results are intriguing, but do not directly address whether annexin A6 may have a role in membrane repair in AD.

Here, we investigate the link between annexin A6, Aβ-induced membrane damage, calcium and calpain dysregulation, DN formation, tau kinase activation, and subsequent phospho-tau accumulation. We demonstrate that DNs have raised resting calcium, elevated calpain activity, increased phosphorylated tau kinases, and accumulation of the amyloid biomarkers p-tau181 and p-tau231, together suggesting that DNs promote an environment of pathological tau phosphorylation and cleavage. We show that the membrane repair protein annexin A6 is expressed in neurons of human and murine brains, and overexpression of annexin A6 in the 5XFAD amyloid mouse model reduces DNs and p-tau181, while dominant-negative annexin A6 increases DNs and p-tau181. Promisingly, recombinant annexin A6 injected into 5XFAD and APP-NLGF knock-in mouse brains shows the ability to bind to the membranes of DNs around amyloid plaques suggesting that, like in muscular dystrophy, annexin A6 protein could be investigated as a therapeutic. These data support the further investigation of Aβ-induced membrane damage as an etiological mechanism of DN formation and AD pathogenesis, and the potential therapeutic use of annexin A6 to mediate membrane repair that would disrupt the link between Aβ and tau pathologies for the prevention of AD.

Materials and methods

Mice

Two lines of 5XFAD mice were used in this study. 5XFAD B6/SJL F1 hybrid on mice was bred in-house by crossing 5XFAD transgenic males to B6/SJL F1 hybrid females and genotyped as described [86]. 5XFAD mice on a C57BL/6 J background were maintained by crossing 5XFAD transgenic males to C57BL/6 J females and genotyped using 5XFAD probes at Transnetyx. APP-NLGF mice on a C57BL/6 J background were obtained from Riken (RBRC06344) and the line was maintained by crossing homozygotes. Genotyping was performed using Riken probes through Transnetyx (Memphis, TN, USA). To obtain 5XFAD;Tau$^{-/-}$ tissue, 5XFAD B6/SJL F1 hybrid males were crossed to Tau$^{-/-}$ females from Jackson Laboratories (strain number 007251). The resulting 5XFAD;Tau$^{+/-}$ males were crossed to Tau$^{-/-}$ females to obtain 5XFAD;Tau$^{-/-}$ animals that were harvested at 9 months of age. Genotyping for tau was performed as described on Jackson Laboratories website and in original reference [25]. Mice were sacrificed by a lethal dose of ketamine/xylazine, followed by transcardial perfusion with 10 ml ice cold 1xPBS containing protease and phosphatase inhibitors. One hemibrain was dissected into hippocampus and cortex which were snap-frozen separately. The other hemibrain was drop fixed in 10% buffered formalin overnight at 4 °C, transferred to 20% w/v sucrose in 1xPBS for 24 hours, and then stored in 30% w/v sucrose in 1xPBS with azide. All animal work was done with the approval of the Northwestern University IACUC, assurance number A3283-01. The number and sex of animals used per experiment is described in detail in the specific methods section of the experiment.

AAV PHP.eB and retro-orbital injections for calcium imaging and calpain sensor

Synapsin-GCaMP6s-ER/K linker-TdTomato (VB230218-1013vfu) and calpain sensor synapsin-Cerulean-PLFAAR-Venus (VB231102-1456esn) were generated and packaged into AAV PHP.eB by Vectorbuilder. For retro-orbital injections, mice were anesthetized in 2.5% isoflurane and 1% oxygen, and then received 100 ul of virus into the retro-orbital sinus, using a 30 gauge needle.

For calcium imaging, five 5XFAD female mice and two non-Tg littermates received $5.5x10^{11}$ viral genomes of syn-GCaMP6s-ERK-TdT at 5–6 months of age and were collected for live imaging 4 weeks later at 6–7 months of age. Twenty-four hours prior to live imaging, mice received intraperitoneal injection of 100 ul of 5 mg/ml MeX04 (HelloBio) in 15% DMSO, 45% propylene glycol, and 40% PBS pH 7.5 24 hours before harvest. Mice were anesthetized with ketamine/xylazine then transcardially perfused with superchilled oxygenated sucrose artificial cerebrospinal fluid (ACSF). One hemibrain was sliced on a vibratome in chilled oxygenated sucrose ACSF solution to 300µm coronal sections. Sections were warmed to 32 °C and equilibrated into oxygenated ACSF, and then cooled to room temperature for imaging. Slices were imaged at room temperature in ASCF for no more than 30 min. Images were collected with a 25x dipping lens on a Nikon A1R Multiphoton with Chameleon Vision titanium sapphire laser tuned to 920 nm for GCaMP6s/TdTomato and 760 nm for MethoxyX04. Images were collected every 2 µm for 50–70 µm z-stacks. In FIJI, maximum projections were generated from the stacks, Regions of interest (ROIs) were drawn around cell bodies and dystrophic neurites, and the ratio of GCaMP6s intensity to TdTomato intensity calculated for each ROI. For each mouse ($n = 5$), 81–131 cell bodies and 407–673 dystrophic neurites from 6 to 9 Z stacks from 3 individual slices were used for quantification. Data are presented as the average for each mouse.

For calpain activity measurement, 5XFAD and non-Tg littermates ($n = 3$) received 1 x 10^{12} viral genomes of Cerulean-PLFAAR-Venus (CFP–PLFAAR–YFP) at 7.5–9.5 months of age and were harvested 5 weeks later for immunofluorescence and biochemistry, as described above. Formalin-fixed brains were sectioned at 30 µm, and incubated with 1:15,000 of 1 mg/ml Thiazine red to label plaques. Imaging was performed on Nikon A1R confocal with a 20x NA 0.75 lens, and images captured in NIS-Elements software (Nikon). The CFP, YFP, and FRET (YFP emission wavelength with CFP excitation) intensities were quantified from single confocal images in FIJI. Three-to-four random cortical fields were used per mouse ($n = 2$) containing 2–11 neuronal soma and 9–64 dystrophic neurites per image for a total of 46 cell bodies and 245 dystrophic neurites.

AAV8 and P0 injections

Synapsin-A6GFP (VB200511-1403pbc), synapsin GFP (VB200603-1246qqd), and synapsin-A6 N32GFP (VB210122-1156evb) AAV plasmids were generated and packaged in AAV 8 serotype by VectorBuilder (Chicago, IL USA). Genomic titer was determined by quantitative PCR. 5XFAD transgene positive males were crossed to SJL/B6 hybrid females in timed matings to generate transgene negative and positive littermates. On P0, each pup in a litter (4 litters per virus, 22–28 pups) was cryo-anesthetized and injected with 2 µl/hemisphere containing 2×10^{11} viral genomes of Syn-A6GFP, or 2×10^{10} viral genomes of Syn-GFP, to compensate for the higher expression of GFP alone. For syn-A6 N32-GFP, 2×10^{10} viral genomes/hemisphere were injected, due to known toxicity of the protein in muscle [108]. All injections were done using a using a 10 µl Hamilton syringe with a 30 gauge replaceable needle, as described in [71]. Pups were returned to the mother and aged to 4.5 months. All 5XFAD transgene positive males were used for analysis (4–6 per AAV).

Recombinant A6-HIS and A6-GFP and stereotaxic injection

Recombinant annexin A6-HIS tagged protein was generated by Evotec SE (Hamburg, Germany) contract research service for protein purification using *E. coli* as described in [29]. The AbVec2.0 vector was used to express A6-GFP intracellularly in HEK293 suspension cells with a 6X-Histidine tag to allow for purification via Ni-NTA chromatography. HEK293 suspension cells were grown with the FreeStyle Expression System (Gibco) and transfections performed using polyethylenimine and OptiPRO SFM (Gibco). Cells were pelleted and lysed in mild detergent M-PER (Thermofisher) containing protease inhibitor and benzonase nuclease. Protein from the lysates was purified via their His-tag using cOmplete Ni-NTA resin (Roche) and dialyzed against PBS, and then quantified on a NanoDrop (Thermofisher)

For stereotaxic injection of recombinant annexin A6-HIS and A6-GFP, 5XFAD and APP-NLGF mice were anesthetized with isoflurane (1.5–2.5%) and 1% oxygen in a stereotaxic apparatus. The lateral ventricle (B-L −0.5; M-L+/–1; D-V −2.5) or the dentate gyrus (B-L −2.5; M-L +/−2.0; D-V −2.2) and overlying cortex (B-L −2.5; M-L +/−2.0; D-V −2.0) were targeted. For A6-HIS, 5XFAD (n=5 males, 5–10 months old) or NLGF mice ($n = 4$, 2 males, 2 females, 9–11 months old) received 0.67 mg/kg into the hippocampus and cortex, or 6.6 mg/kg into the ventricle. Both injection targets produced similar subcellular localization of protein with different anatomic distribution, For A6-GFP, 5XFAD ($n = 2$ males, 11 months old) or NLGF mice ($n = 3$, 2 male, 1 female, 9–10 months old) received 0.45–0.9 mg/kg into the

hippocampus and overlying cortex. Animals were sacrificed and tissue harvested 3–5 hours later, as described, and tissue sectioned and stained for imaging. 3–5 hours was chosen as a time frame that allowed protein to diffuse and bind to targets, but before it was degraded appreciably.

Immunofluorescence and image quantification

10% formalin-fixed hemibrains were sectioned at 30 µm on a freezing sliding microtome and collected in cryopreserve (30% w/v sucrose, 30% ethylene glycol in 1X PBS) then stored at – 20 °C. If required, antigen retrieval was performed for 45 min at 80 °C in 0.1M sodium citrate, in TBS, and then allowed to cool for 15 min before rinsing well and proceeding with staining. Sections were blocked in 5% normal donkey serum in TBS with 0.1% Triton-X 100 (TBS-T) and then primary antibodies added in 1% BSA in TBS-T at 4 °C overnight. Primary antibody concentrations can be found in Table 1. Following washes, sections were incubated for 2 hours at room temperature with 1:750 dilutions of Alexa Fluor 405, 488, 568, or 647 conjugated donkey anti-mouse, goat, chicken, rat, or rabbit secondary antibodies, as appropriate, along with the following stains: 300 nM DAPI, and 1:15,000 dilution of 1 mg/ml Thiazine Red (ThR) or MethoxyX04 (MeX) (HelloBio). All secondary antibodies were obtained from ThermoFisher Scientific, except donkey anti-chicken 405, 488, and 647 were from Jackson Immunologicals (West Grove, PA, USA) and donkey anti-rat 568 from Abcam (Waltham, MA USA). Sections were mounted with Prolong Gold (Molecular Probes). For protein localization, images were captured from 2–3 sections per mouse, 2–3 mice per sex and genotype, comprising male and female mice between 6 and 9 months of age, on a Nikon A1R confocal microscope using 60x objective.

For quantification of LAMP1 and p-tau181 in dystrophic neurites, and Iba1 and GFAP quantification around plaques,

Table 1 List of primary antibodies used for immunoblotting and immunofluorescence

Immunoblot antibodies				
Protein	Company	cat #	conc	Species
Annexin A6	Abcam	Ab199422	1:5000	Rabbit
GFP	Abcam	Ab5450	1:1000	Goat
APP 6E10	Biolegend	#803001	1:1000	Mouse
β-tubulin	Gift of Nick Kannan	TuJ1 clone	1:10:000	Mouse
FLAG	ProteinTech	80010-1-RR	1:1000	Rabbit

Immunofluorescence antibodies					
Protein	Company	cat #	conc	Species	Antigen retrieval
Iba1	Novus	NB100-1028	1:300	Goat	
Annexin A6	Abcam	Ab199422	1:300	Rabbit	AR needed
GFAP	Abcam	Ab4674	1:2000	Chicken	
BACE1	Abcam	Ab108394	1:300	Rabbit	
BACE1	Vassar Lab	clone 3D5	1:300	Mouse	AR needed
hAPP N-term	Gift of Virginia Lee	karen	1:2000	Goat	
APP C-term Y188	Abcam	Ab32136	1:2000	Rabbit	
Aβ42	Invitrogen	#700254	1:1000	Rabbit	
NeuN	Millipore	Abn91	1:1000	Chicken	
NeuN	Millipore	Mab377	1:200	Mouse	
Aβ	Gift of Elan	3D6	1:1000	Mouse	
LAMP1	DSHB	1D4B clone	1:1000	Rat	Not AR compatible
p-tau 181	Cell signaling	#12885	1:300	Rabbit	
p-tau 231	Abcam	ab151559	1:500	Rabbit	
p-JNK	Cell signaling	#9255	1:500	Mouse	
p-CaMKII	Abcam	ab5683	1:300	Rabbit	
tau	Gift of Nick Kannan	tau5	1:300	Mouse	
anti-HIS	Cell signaling	#12698	1:500	Rabbit	
Annexin A1	Abcam	ab214486	1:300	Rabbit	AR needed
Annexin A2	Abcam	ab189473	1:1000	Rabbit	AR needed
GFP	Abcam	Ab5450	1:5000	Goat	

three sections between Bregma −1.58 mm and Bregma −2.54 mm were stained and imaged per mouse. Images were acquired on a Nikon Ti2 Eclipse widefield microscope with a 10x objective, using the NIS-Elements software high content method to capture and tile whole sections. All image acquisition settings were maintained the same between treatment groups and genotypes. For image analysis, ROIs were drawn in cortex and hippocampus. Using the General Analysis tool, thresholding was set to distinguish Aβ42, LAMP1, MethoxyX04, Thiazine Red, and p-tau181 positive regions, and then, the percent area covered by each stain from the hippocampal or cortical ROI was calculated. Using the same sections, thresholding in the General Analysis tool was used to define sub-ROIs that correspond to individual plaques having both Aβ42 and LAMP1 or p-tau181 and Thiazine red positive pixels within cortical and hippocampal ROIs. The General Analysis tool was used to measure area covered by Aβ42 and by LAMP1, or p-tau181 and ThR or p-tau181 and MeX in a given sub-ROI (plaque), and the ratio between LAMP1:Aβ42, p-tau181:ThR or p-tau181:MeX was calculated in Excel. 615–1393 plaques were analyzed per mouse in cortex and 210–527 plaques in hippocampus. Four-to-five male mice per genotype/treatment group were analyzed, using three sections per mouse.

For measurement of area of GFP-positive (GFP+) dystrophic neurites, three sections from each mouse (5 A6-GFP injected and 5 GFP injected) were imaged on a Nikon A1R confocal with a 60x objective. The section of cortex directly above hippocampus to the top of layer 5 of the cortex was imaged, and a tiled imaged of multiple fields (8 × 4) was generated to create a single image 1474.36 by 753.23 microns. Within this region, Nikon NIS-Elements software was used to threshold GFP+ structures, excluding cell bodies based on size, and the size of each GFP+ structure was measured. 1761–4941 GFP+ dystrophic neurites were measured per mouse.

Human tissue

30 µm floating sections of hippocampal tissue from 3 individuals with autopsy confirmed AD pathology (1 male, 2 female, ADNC high—A3, B3, C3), and 3 non-cognitively impaired age-matched controls (2 male, 1 female) were obtained from the brain bank of the Mesulam Center for Cognitive Neurology and Alzheimer's Disease at Northwestern University. Immunofluorescence was performed as described for mice, except that sections were blocked in 10% normal donkey serum, with 2% BSA in TBS with 0.1% TBS-T and primary antibodies added over night in 2% normal donkey serum with 2% BSA in TBS-T at 4 °C. As a final step before mounting, sections were incubated 7 min in TrueBlack (#23014 Biotium) diluted 1:40 in TBS.

HEK293 and SH-SY5Y cell culture (supplemental figures)

HEK293 cells were obtained from ATCC and cultured in DMEM with glucose, 10% fetal bovine serum, and 1% penicillin/streptomycin all from ThermoFisher scientific. Calpain 1 small subunit expression construct was obtained from Origene (RC212322) and calpain 1 large subunit was obtained from Addgene (60941). Both plasmids, along with UBC-CFP–PLFAAR–YFP from VectorBuilder, were prepared with Machery Nagel MuceloBond Xtra maxi kits and transfections performed with Lipofectamine 2000 (Invitrogen). After 24 h, cells were lysed in RIPA buffer and sonicated, and protein concentration was quantified using BCA Assay (Pierce). 10 µg of protein was boiled 10 min in 1x LDS sample loading buffer, and immunoblotting performed as described below. For FRET imaging, cells were plated on coverslips, and then, 24 h after transfection were fixed in 4% paraformaldehyde, mounted on slides, and imaged, as described previously for FRET. SH-SY5Y cells were obtained from ATCC and cultured in DMEM with glucose, 10% fetal bovine serum, and 1% penicillin/streptomycin, all from ThermoFisher scientific. For imaging, cells were plated on coverslips coated with laminin in media containing retinoic acid to induce differentiation. GCaMPs-TdTomato was transfected into SH-SY5Y cells using Lipofectamine 2000. Cells were imaged on 25x dipping lens on a Nikon A1R Multiphoton with Chameleon Vision titanium sapphire laser tuned to 920nm for GCaMP6 s/TdTomato, in Ringer's with calcium (155 mM NaCl, 4.5 mM KCl, 5 mM HEPES, 10 mM D-Glucose, 1 mM $MgCl_2$, and 2 mM $CaCl_2$). Images were captured every 5 s for 5 min, with 90 mM KCl in Ringer's with calcium infused in after 1 min of imaging to depolarize cells. Calcium levels were quantified using FIJI as described above, taking the ratio of GCaMP6 s to TdTomato in each cell.

Immunoblotting

Snap frozen cortices and hippocampi were homogenized in 1000 µl or 300 µl, respectively, of T-PER Tissue Protein Extraction Reagent (ThermoFisher), supplemented with protease inhibitors (Calbiochem) and Halt Phosphatase Inhibitor Cocktail (Thermo Scientific). Protein concentration was quantified using BCA Assay (Pierce). 20 µg of protein was boiled 10 min in 1X LDS sample loading buffer, and then separated on 4–12% NuPage Bis-Tris Bolt gels (FisherScientific) in MES buffer (FisherScientific). Protein was transferred to nitrocellulose membrane using BioRad Trans_Blot Turbo Transfer System, then stained with 0.1% Ponceau in 5% w/v acetic acid, and imaged. Membrane was rinsed well, blocked, and then probed with the following primary antibodies: anti-APP (6E10, BioLegend 803001, 1:2000),

anti-Annexin A6 (Abcam ab 1:5000), anti-β-tubulin (TuJ1, gift of Dr. Nicholas Kanaan, 1:10,000), anti-FLAG (ProteinTech, 80010-1-RR, 1:1000), anti-GFP (Abcam ab5450, 1:1000) followed by HRP-conjugated anti-mouse, anti-rabbit, or anti-goat secondary antibody (Vector Laboratories 1:10,000). 5% milk was used as a blocking agent. Blots were visualized using chemiluminescence (BioRad Clarity), and band intensities measured using a BioRad ChemiDoc Touch Imaging System and then quantified with the ImageLab software (BioRad). Signal intensities were normalized to that of tubulin. Statistical analyses were performed as described below.

Protein schematics

Protein ribbon diagrams were generated using Swiss-PdbViewer using solved crystal structures of human annexin A6 with phosphorylation mimicking mutant T356D (1M9I), www.rcsb.org.

Statistics

Student's two-tailed t test and ANOVA were done using InStat software (GraphPad Software, Inc., San Diego, CA) to compare means of the various genotypes, genders, and treatment groups. * $0.05 > p > 0.01$ ** $0.01 > p > 0.001$ *** $0.001 > p > 0.0001$; Error bars = S.E.M.

Results

Dystrophic neurites have elevated resting calcium

Since we hypothesized that contact with amyloid plaques disrupts the membrane of nearby axons leading to calcium influx and subsequent disruption of kinases and phosphatases, microtubule-based transport, and ultimately neuronal function, we wanted to assess steady-state resting calcium levels in DNs. To do so, we generated a sensor fusion protein, GCaMP6s-TdT, consisting of the highly sensitive calcium sensor GCaMP6s [16] fused to calcium insensitive TdTomato (TdT), which was included to normalize for sensor protein expression (Fig. 1A). Our calcium sensor allowed us to measure steady-state resting calcium, rather than calcium change over time, as is more commonly done using GCaMP variants alone. We inserted a stiff α-helical 30 residue ER/K linker between GCaMP6s and TdT to increase the distance between the two fluorescent proteins for minimizing FRET interactions [104, 109]. We verified the calcium responsiveness of GCaMP6s-TdT by measuring GCaMP6s:TdT fluorescence ratio during depolarization. SH-SY5Y cells were transfected with the neuron-specific human synapsin-GCaMP6s-ER/K-TdT (hSyn-GCaMP6s-ER/K-TdT) plasmid, differentiated with retinoic acid, and then imaged using multiphoton microscopy while being depolarized with 90 mM KCl. We observed that the ratio of GCaMP6s:TdT fluorescence was increased by about tenfold in depolarized cells compared to non-depolarized cells (Supplemental Fig. 1A, B).

To assess resting calcium levels *in vivo* in DNs, we packaged syn-GCaMP6s-ER/K-TdT into AAV PHP.eB, which crosses the blood–brain barrier when injected intravenously [14, 55]. 6–7 month-old 5XFAD mice were retro-orbitally injected with syn-GCaMP6s-ERK-TdT AAV and brains collected 5 weeks later and sliced for live multiphoton microscopy imaging. To label plaques in live brain slices without relying on antibody staining, mice received a single IP injection of the brain-penetrant small molecule amyloid dye, Methoxy-X04, 1 day before harvest. DNs around dense core plaques labeled with Methoxy-X04 showed more green GCaMP6s on average than neuronal cell bodies (Fig. 1B). The GCaMP6s:TdT fluorescence ratio was quantified for individual DNs and neuronal soma in single 50–70 mm z-stack images (Fig. 1C) and as the average DN and soma ratios per mouse (5 mice, 6–9 DN and soma images each from 3 slices per mouse; Fig. 1D). Overall, DNs showed a significant increase in GCaMP6s:TdT ratio in compared to cell bodies, indicating increased resting calcium levels in DNs. Live multiphoton microscopy imaging of 5XFAD brain slices without syn-GCaMP6s-ER/K-TdT AAV injection demonstrated green- and red-channel autofluorescence in plaque cores and puncta in neuronal soma and surrounding neuropil (Supplemental Fig. 1C). We verified that the formation of DNs is not dependent upon the intraneuronal expression of human APP from the 5XFAD transgene by performing co-staining with a human-specific N-terminal APP antibody [112] and an APP antibody that recognizes both mouse and human APP (rabbit monoclonal Abcam ab32136), or an antibody recognizing BACE1, demonstrating that not all dystrophic neurites contain human APP (Supplemental Fig. 2). Rather, DNs appear to form as a response to amyloid plaques in close proximity.

Dystrophic neurites have increased calpain activity

Since calcium levels control the activity of the protease calpain, which is known to cleave tau potentially leading to the generation of aggregation-prone toxic fragments [11, 91], we also developed a calpain sensor to assess calpain activity in DNs. The calpain sensor construct (CFP–PLFAAR–YFP) consists of cerulean fluorescent protein (CFP) fused to mVenus yellow fluorescent protein (YFP) via a calpain cleavage site linker referred to by its amino-acid sequence, PLFAAR (Fig. 2A) [81]. To test the specificity of our calpain sensor, we expressed it in HEK293 cells with or without co-expression of the calpain 1 large and small subunits. Cleavage of

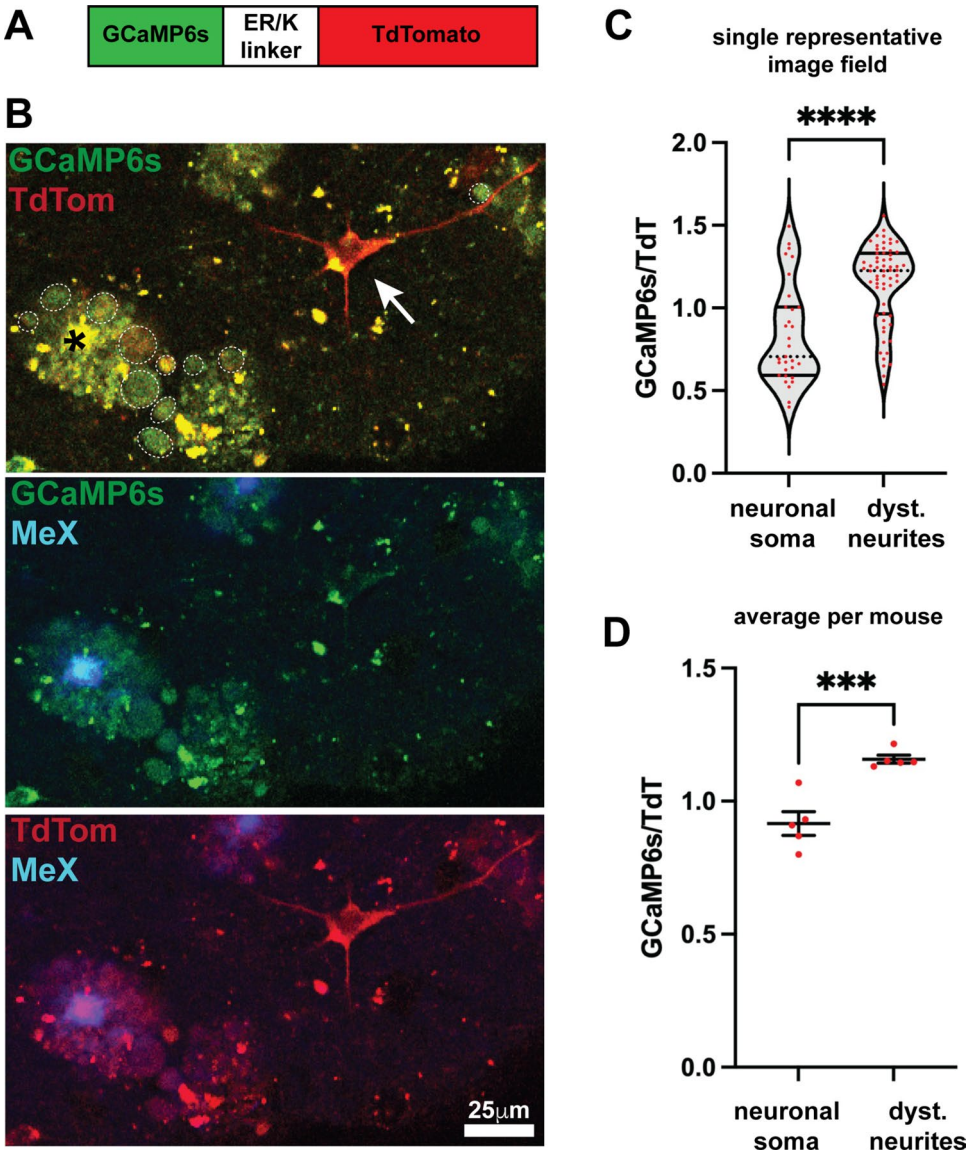

Fig. 1 Resting calcium levels are elevated in dystrophic neurites of 5XFAD mice. **A** Schematic of ratiometric calcium sensor GCaMP6s-ERK-TdTomato. **B** 300 µm live slices of 5XFAD (N = 5) mice injected with AAV PHP.eB syn-GCaMP6s-ERK-TdT were imaged on a Nikon A1R confocal multiphoton microscope at 25x. Upper panel of B shows an example of a neuronal soma with low GCaMP6s fluorescence (arrow) and dystrophic neurites with higher GCamP6s fluorescence (dotted circles). Lower panels show MethoxyX04 (MeX) marking dense core amyloid plaques and the fluorescence of GCaMP6 s (middle panel) or TdTomato (lower panel) independently. Imaging of brain slices from 5XFAD mice without GCaMP6s-ERK-TdTomato expression indicated that bright signals from plaques and puncta are autofluorescence of live tissue (Suppl. Fig. 1C). **C**, **D** For each z stack (n = 6–9 per mouse, from 3 different slices, 5 mice), the ratio of GCaMP6s:TdT was quantified in neuronal soma and dystrophic neurites using FIJI. **C** All neuronal soma and dystrophic neurites from one representative z stack are shown, indicating a significant increase in ratio in dystrophic neurites, but with wide variation (image shown in Sup. Fig 1D). Dotted black line represents median, solid black lines represents quartiles, and red points indicate individual cells or dystrophic neurites. **D** The average GCaMP6s:TdT ratio per mouse (n = 6–9 z-stacks per mouse, from 3 different slices, 5 mice) is shown, demonstrating a significantly increased GCaMP6s:TdT ratio, but with decreased variation. Two tailed Students t test, ****$p < 0.0001$, ***$p < 0.001$. Red points represent individual mice, with mean and SEM

CFP–PLFAAR–YFP was observed only when the calpain subunits were co-expressed, demonstrating specific detection of calpain activity (Supplemental Fig. 3A). A negative control calpain sensor with a GGGGS linker that cannot be cleaved by calpain, CFP-GGGGS-YFP, remained full length following co-expression of the calpain 1 large and small subunits (Supplemental Fig. 3A).

Next, we used our calpain sensor to assess calpain activity *in vivo* in DNs of 5XFAD mice. CFP–PLFAAR–YFP under control of the synapsin

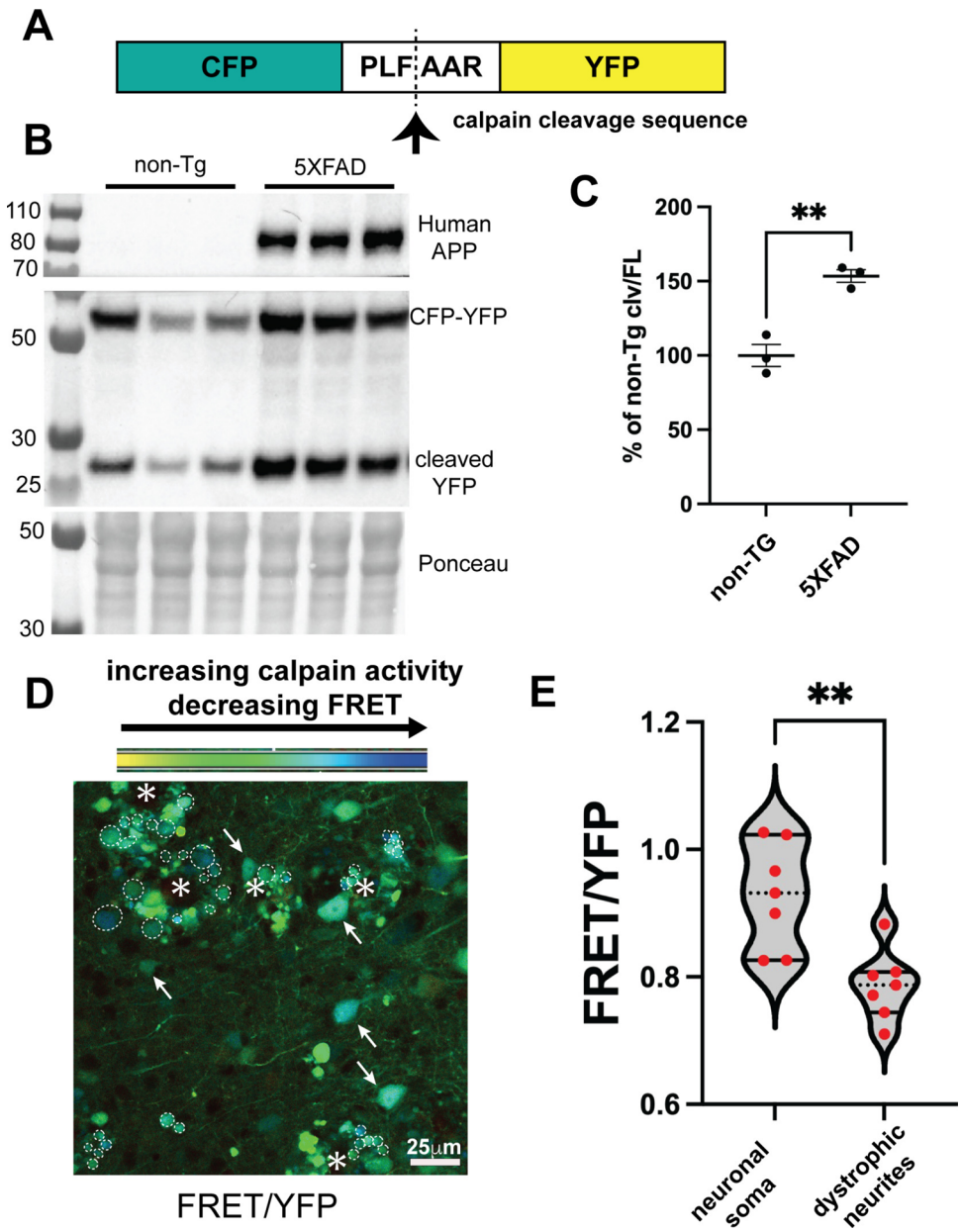

Fig. 2 Calpain activity is elevated in dystrophic neurites of 5XFAD mice. **A** Schematic of calpain sensor CFP–PLFAAR–YFP. Arrow indicates calpain cleavage site. **B**, **C** At 6–7 months of age, 5XFAD mice and non-transgenic littermates (n=3 each genotype) received a retro-orbital injection of AAV PHP.eB syn-CFP–PLFAAR–YFP. After 5 weeks of expression, brains were collected and immunoblot analysis performed, which indicated significantly elevated ratio of cleaved to full-length CFP–PLFAAR–YFP in 5XFAD mice compared to non-Tg mice. **D**, **E** Using FIJI, FRET and YFP intensity were measured in neuronal soma (arrows) and dystrophic neurites (dotted circles). **E** The ratio of FRET:YFP was significantly decreased in dystrophic neurites compared to neuronal cell bodies, indicating an increase in calpain activity in dystrophic neurites. For (**E**), 3–4 random cortical fields were used per mouse ($n = 2$) containing 2–11 neuronal soma and 9–64 dystrophic neurites per image for a total of 46 cell bodies and 245 dystrophic neurites. Each red data point represents the ratio in a cortical field. Dotted black line represents median and solid black lines represent quartiles

promoter (syn-CFP–PLFAAR–YFP) was packaged into AAV PHP.eB and retro-orbitally injected into 7-month-old 5XFAD mice and non-transgenic (non-Tg) littermates that were aged 5 weeks and brains harvested for immunoblot analysis of brain homogenates and FRET in brain sections. By immunoblot, we observed significantly increased cleavage of CFP–PLFAAR–YFP in 5XFAD compared to non-Tg mice, indicating greater calpain activity in the presence of amyloid pathology (Fig. 2B and C). To determine if increased CFP–PLFAAR–YFP cleavage occurred in DNs, we quantified FRET between CFP and YFP in neuronal soma and DNs of fixed brain sections from the same mice. First, we validated effective FRET between CFP and YFP in fixed HEK293 cells and fixed 5XFAD brains by photobleaching the acceptor (YFP) and observing an increase in fluorescence of the donor (CFP) and a decrease of FRET (Supplemental Fig. 3B and C, respectively). Finally, we determined FRET:YFP ratio (Fig. 2D, E) in neuronal soma and DNs of 5XFAD mice expressing CFP–PLFAAR–YFP, demonstrating that FRET was decreased in DNs compared to the cell body. Images depicting a scaled ratio of FRET:YFP intensity visualized differences in calpain activity between neuron cell bodies and DNs (Fig. 2D). CFP images, which showed better resolution of individual DNs and cell bodies, were used to select regions of interest for quantification. Thiazine red staining marked plaque locations, so only DNs in the proximity of plaques were selected (Supplemental

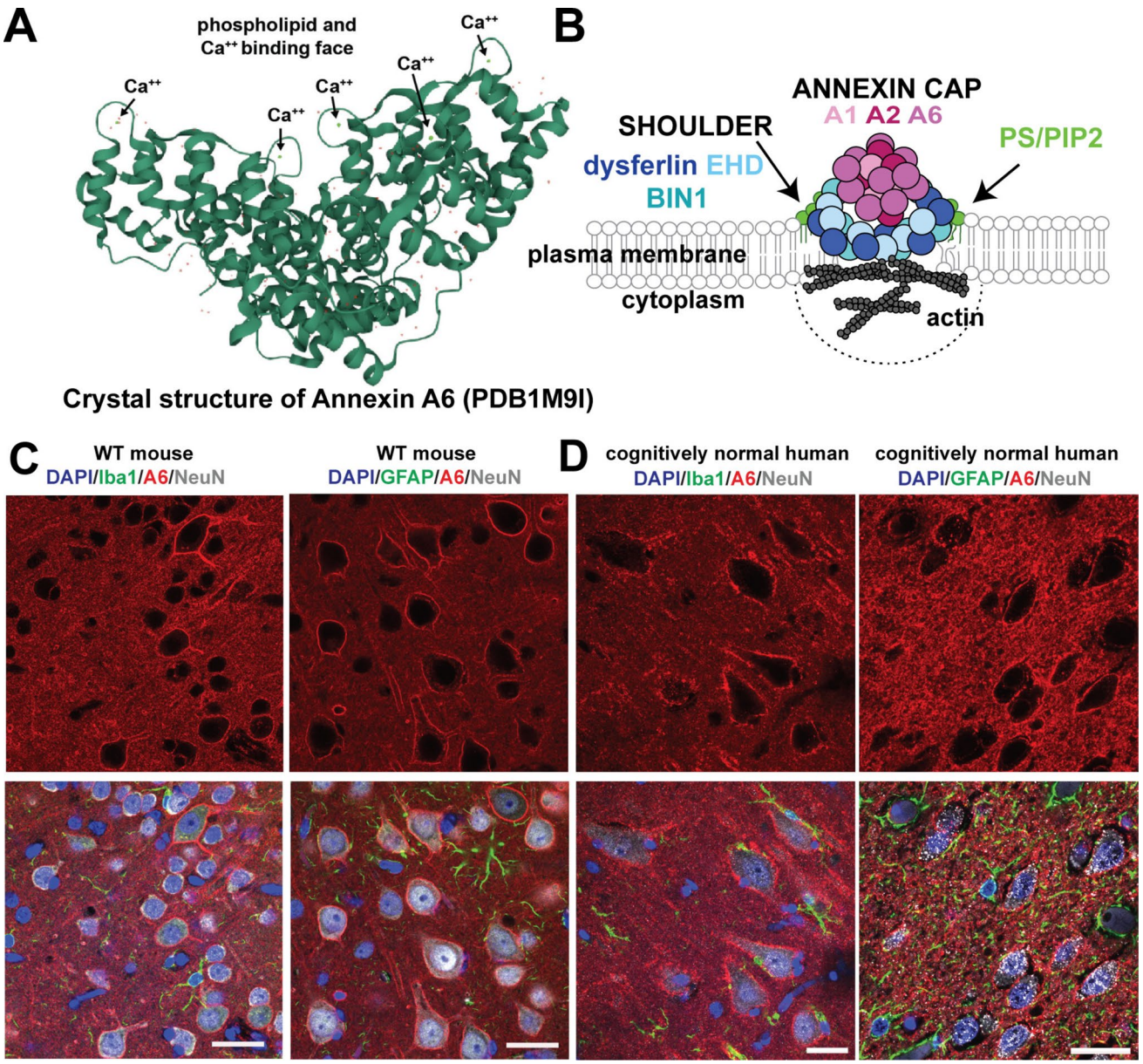

Fig. 3 Annexin A6 localizes to neuronal plasma membrane in mouse and human brain. **A** Annexin A6 crystal structure. Arrows labeled "Ca^{++}" point at green dots that represent bound calcium molecules. **B** Schematic of annexin A6 repair cap complex following membrane injury. PS, phosphatidylserine; PIP2, phosphatidylinositol biphosphate. **C, D** Wild-type (WT) mouse (**C**) and cognitively normal human (**D**) brain sections immunostained for annexin A6 (red), NeuN (gray), Iba1 (green), GFAP (green), and DAPI (blue)

Fig. 3D). Together, these results show that calpain activity is elevated in DNs, which may contribute to pathologic fragmentation of tau.

Membrane repair protein Annexin A6 localizes to the plasma membrane of neurons in normal brain

We hypothesized that DNs form due to membrane damage from contact with plaque-associated Aβ, which leads to increased calcium influx and calpain and kinase activation, as well as microtubule depolymerization, impaired axonal transport, and pathologic tau generation. If true, then enhanced membrane repair should reduce Aβ-associated DNs and pathologic tau. Annexin A6 functions to repair damage to plasma membranes in cells, especially those that undergo mechanical stress, such as muscle cells, or large cells with a high surface area, like neurons. We therefore investigated the possibility of enhancing membrane repair with annexin A6 to decrease the formation of dystrophic neurites.

First, we determined the cellular localization of endogenous annexin A6 in the brain using a specific antibody (rabbit monoclonal Abcam ab199422). We immunostained mouse and human brain sections and found annexin A6 localization in neurons, but not microglia or astrocytes, of wild-type mice (Fig. 3C) and cognitively normal aged humans (Fig. 3D). Most striking is the strong annexin A6 localization at the plasma membrane in both human and murine neurons.

Annexins A1 and A2 play secondary roles in membrane repair in muscle, adding to the repair cap after the recruitment of annexin A6 (Fig. 3B), and therefore may participate in membrane repair in neurons. To investigate this, we investigated single-cell RNA sequencing data from the Human Protein Atlas (https://www.proteinatlas.org/), which indicates high levels of annexin A6 in neurons. Conversely, annexins A1 and A2 are found in endothelial cells and pericytes in the brain, with very low levels in some excitatory neurons (A1) and inhibitory neurons (A2) (Supplemental Fig. 4A–C). Our immunostaining confirmed predominant localization of annexin A2 in vasculature and choroid plexus with no visible staining in neurons (Supplemental Fig. 4D, E), as previously reported [122]. Together, our results demonstrate that annexin A6 strongly localizes to neuronal membranes, and is a prime candidate for neuronal membrane repair in the brain.

In the presence of amyloid plaques, endogenous and overexpressed annexin A6 localizes to dystrophic neurites

The strong prevalence of annexin A6 over A1 and A2 in neurons, along with the observation that A6 localizes to sites of injury in neurons [29] and is the key factor for initiation of membrane repair in myofibers [30, 31], led us to focus on annexin A6 expression as a potential approach for reducing Aβ-associated membrane damage, DN formation, and pathologic tau generation in AD. To test whether annexin A6 could reduce DNs, we used a somatic brain transgenesis approach [71] to express syn-GFP AAV or syn-A6-GFP in the neurons of mice throughout their lifetime. On P0, we performed intracerebroventricular injections of pups with either syn-GFP AAV or syn-A6-GFP AAV8, then aged them to 4.5 months and collected brain tissue. Immunoblot analysis showed that A6-GFP was expressed ~8 fold higher than endogenous A6 (Suppl. Fig. 5 A, B), which mice tolerated well with no obvious ill effects, and protein expression was widespread through the cortex and hippocampus (Suppl. Fig. 5C). GFP fluorescence revealed A6-GFP expression in neurons and DNs (Fig. 4A). A6-GFP colocalized with BACE1 in DNs, indicating A6-GFP reached the correct location to repair potential membrane damage in DNs. AAV-mediated A6-GFP overexpression recapitulated the localization of endogenous A6, which was also found in membranes of neurons and DN (marked by BACE1 or APP) in 5XFAD transgenic (Fig. 4B) and APP-NLGF knock-in (Fig. 4C) amyloid model mice, and brains from AD patients (Fig. 4D, E) where it could play a role in amyloid-induced membrane repair.

AAV-mediated expression of annexin A6 reduces dystrophic neurites

To determine the effects of annexin A6-GFP on amyloid pathology and DN formation, brain sections from A6-GFP or GFP-alone transduced mice were stained with antibodies against Aβ42 and LAMP1, the latter recognizing lysosomal and late endosomal compartments as well as autophagic organelles that accumulate to high levels in DNs, making it a commonly used DN marker [20, 21, 46] (Fig. 5A). We used Nikon NIS-Elements software to define each plaque and its associated DN halo and determine the ratio of the respective areas stained for LAMP1 and Aβ42 (Fig. 5B). Smaller amyloid plaques grow at faster rates compared to larger plaques and have proportionally greater amounts of neuritic dystrophy [20], so we stratified plaques according to size, based on staining with an anti-Aβ42 antibody, before averaging LAMP1:Aβ42 ratios. As expected, smaller plaques had a higher LAMP1:Aβ42 ratios than larger plaques (Fig. 5B). Importantly, we observed a significant decrease of the LAMP1:Aβ42 ratio of smaller plaques in the hippocampus and cortex of 5XFAD brains injected with A6-GFP AAV compared to those injected with GFP AAV (Fig. 5B). Smaller plaques exhibit the most rapid growth and cause the greatest neurotoxicity [20], so reducing DNs around smaller plaques is likely to have beneficial effects. The distribution of plaque sizes was equivalent in A6-GFP and GFP expressing animals (Suppl. Fig. 5D). The total percent area positive for LAMP1 in the cortex was significantly decreased in A6-GFP AAV-injected 5XFAD brains, while that of Aβ42 was unchanged (Fig. 5C), indicating that A6-GFP specifically reduced DNs with minimal effects on Aβ deposits.

Using higher magnification confocal microscopy images, we observed that the area of individual GFP-positive DNs was significantly reduced in A6-GFP AAV-injected mice compared to those injected with GFP AAV (Fig. 5D). A6-GFP did not affect microglia or astrocytes around plaques, as the ratio of microglial marker Iba1 and astrocyte marker GFAP to the amyloid stain MeX04 in the area within 15μm of the plaque core was unchanged (Fig. 5E). Together, these results strongly suggest that annexin A6 overexpression reduces the formation of DNs, likely via its membrane repair function, but does not affect Aβ pathology.

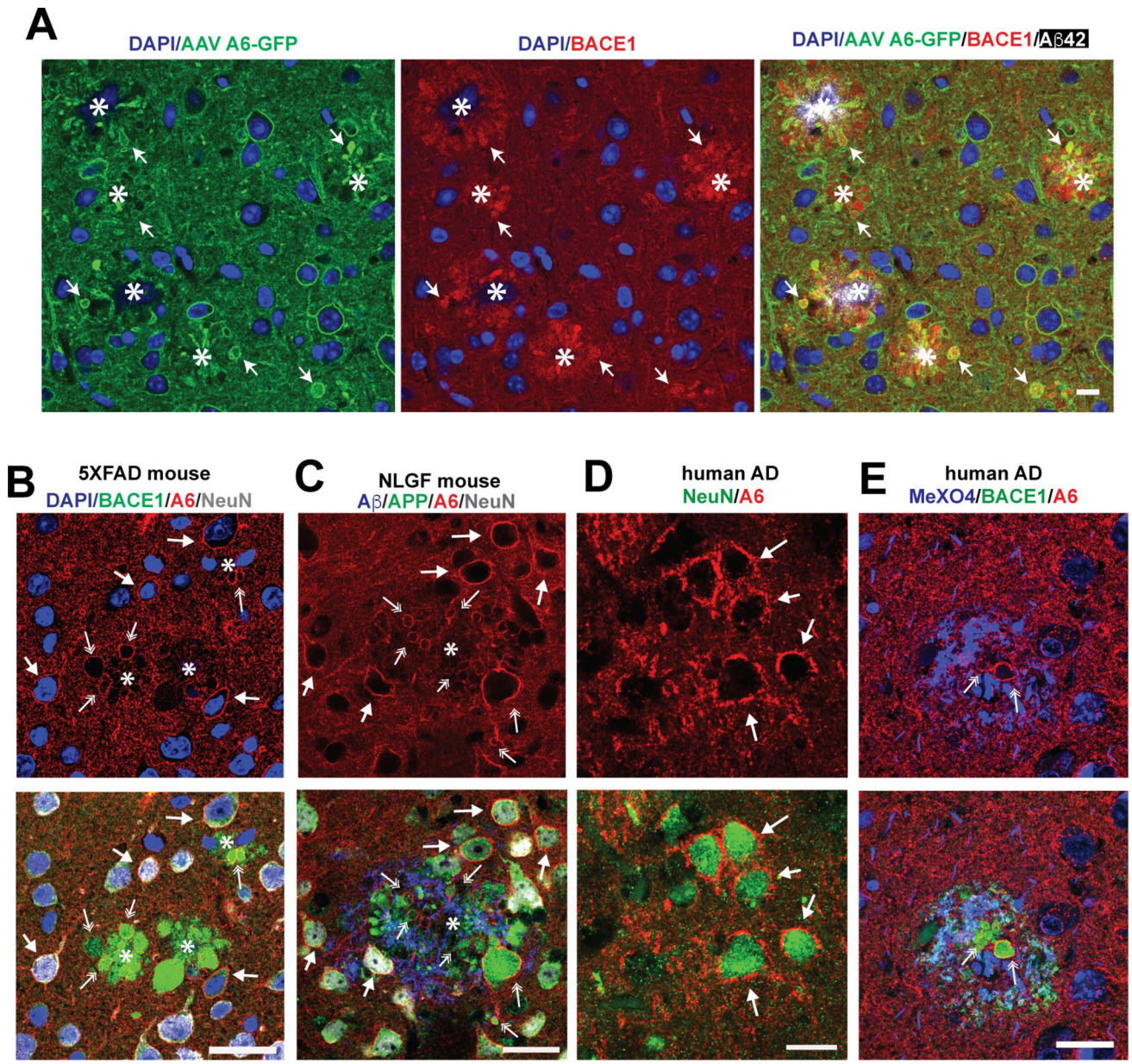

Fig. 4 Overexpressed and endogenous A6 localizes to dystrophic neurite membranes. **A** Cortical section of 5XFAD mouse transduced with AAV expressing A6-GFP driven by the neuron-specific synapsin promoter and immunostained for A6-GFP (anti-GFP, green), BACE1 (red), Aβ42 (white), and DAPI (blue) shows A6-GFP localized to membranes of neuron soma and BACE1+ DNs (arrows); *plaques; Bar=10μm. **B**, **C** 5XFAD (**B**) and APP-NLGF (**C**) cortical mouse brain sections immunostained for annexin A6 (red), BACE1 (green), APP (green), Aβ (blue), NeuN (gray), and DAPI (blue). We used the APP-NLGF knock-in mouse model of amyloid pathology to validate results obtained with 5XFAD mice. **D**, **E** Human AD hippocampal brain sections immunostained for annexin A6 (red), BACE1 (green), MeX04 (amyloid stain; blue), and NeuN (green). *plaque cores; double arrows, DNs; arrows, neurons. Bars=10μm (A), 25μm B-E)

Tau phosphorylated at Thr181 accumulates in dystrophic neurites and is reduced by annexin A6 overexpression

Previous work has suggested that plaques and associated neuritic dystrophy play a key role in pathologic AD tau seeding and spreading [53, 72, 89]. When tau seeds purified from human AD brain are injected into amyloid mouse model brains, tau spreading, as detected by antibody AT8, positively correlates with the amount of plaques and the degree of neuritic dystrophy around plaques, with AT8 positivity appearing specifically in DNs rather than cell bodies [53, 72, 89]. CSF and plasma biomarkers p-tau181 and p-tau231 correlate significantly

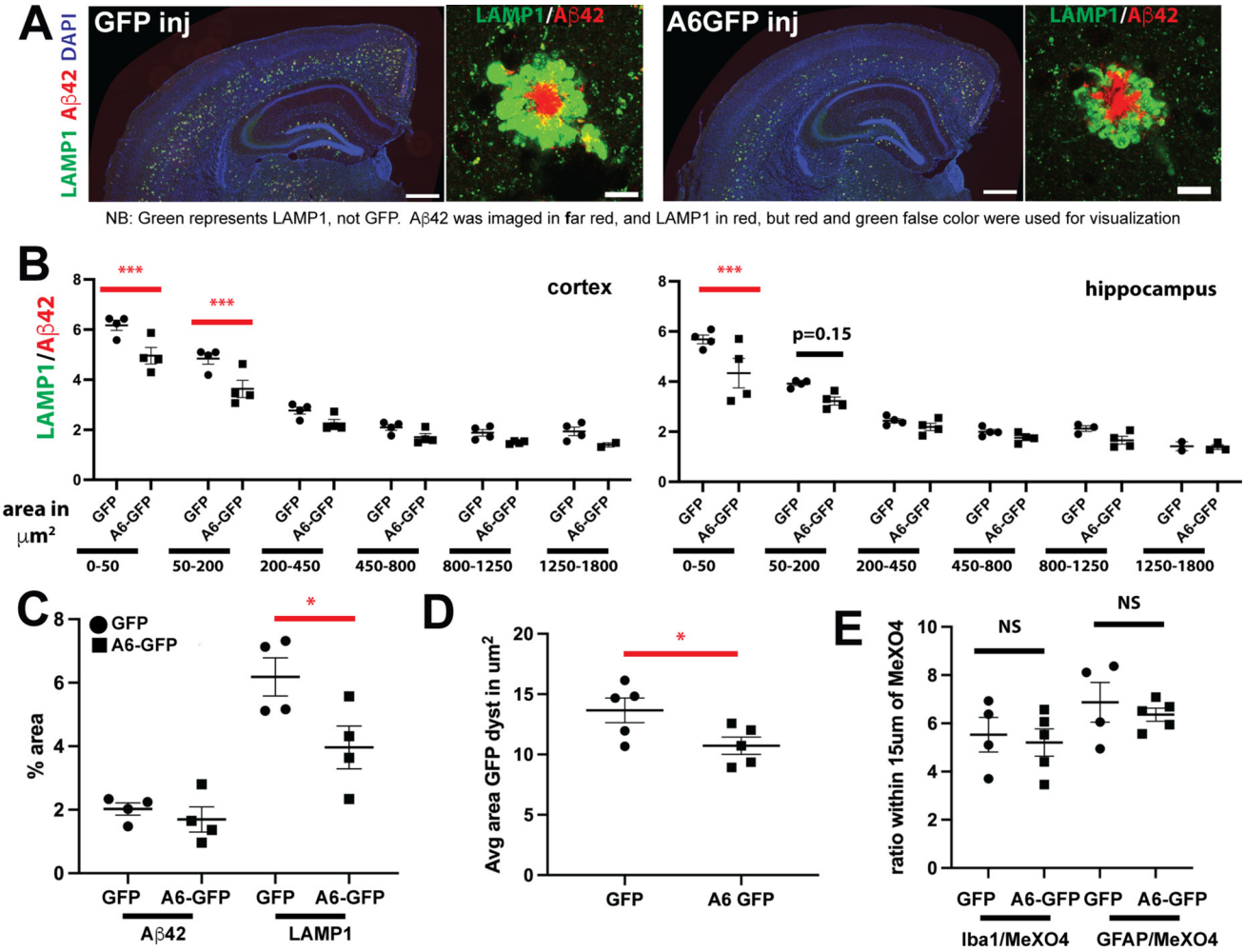

Fig. 5 Annexin A6-GFP reduces dystrophic neurites without affecting Aβ deposits or glia in 5XFAD brain. **A** Coronal brain sections of 5XFAD mice transduced with AAV expressing GFP alone or A6-GFP driven by the neuron-specific synapsin promoter and immunostained for Aβ42 (red), LAMP1 (green), and DAPI (blue). Note the smaller LAMP1+ dystrophic neurite halo surrounding the amyloid plaque in A6-GFP expressing 5XFAD mice (far right). Bars=500 µm, left panels; bars=10 µm, right panels. **B** LAMP1/Aβ42 ratio of amyloid plaques in cortex (left) and hippocampus (right) of 5XFAD mice expressing GFP alone ($n = 4$) or A6-GFP ($n = 4$) binned by plaque core area with the indicated ranges in µm^2. Expression of A6-GFP significantly reduced LAMP1/Aβ42 ratio in smaller, faster growing plaques in the size ranges of 0–50 and 50–200 µm^2. ***, $p < 0.001$. **C** %Aβ42+ (left graph plots) and %LAMP1+ (right graph plots) areas are unchanged and significantly reduced, respectively, in 5XFAD mice expressing A6-GFP compared to GFP alone. *$p < 0.05$. **D** Endogenous GFP fluorescence was imaged using confocal microscopy, and ImageJ used to quantify size of GFP+ DNs. Average area of GFP+ DNs is significantly reduced in 5XFAD mice expressing A6-GFP compared to GFP alone. *, p<0.05. **E** Ratios of Iba1 (left graph plots) and GFAP (right graph plots) to amyloid as measured by MeX04 staining within 15 µm of plaque cores are unchanged in 5XFAD mice expressing A6-GFP compared to GFP alone, indicating A6-GFP causes no change in microglia or astrocytes near plaques. In all graphs, each point represents an individual animal

with Aβ pathology and predict AD onset years in advance [6, 7, 79, 107]. We therefore hypothesized that these early markers of Aβ pathology would be present in DNs. Indeed, using specific antibodies for p-tau181 (Fig. 6A, C) and p-tau231 (Fig. 6D), we observed that p-tau181 and p-tau231 accumulated in DNs of 5XFAD and APP-NLGF brains, as shown by colocalization with LAMP1 and/or BACE1. No signal for p-tau181 or p-tau231 was detected in 5XFAD;Tau$^{-/-}$ brain (Fig. 6A, D). As we show here, and others have reported [92, 96], amyloid mouse models still have robust DN formation in the absence of tau, clearly indicating that tau is not required for generating DNs. Interestingly, p-tau231 and p-tau181 had different localization patterns. P-tau181 appeared in mossy fibers and DNs in both wild-type and 5XFAD mice (Suppl. Fig. 6A, B), while p-tau231 localization was more somato-dendritic (Suppl. Fig. 6C, D). These observations suggest that p-tau181 is predominantly found in axonal compartments compared to p-tau231. However, p-tau231 does appear in DNs, but less frequently than p-tau181. Moreover, these

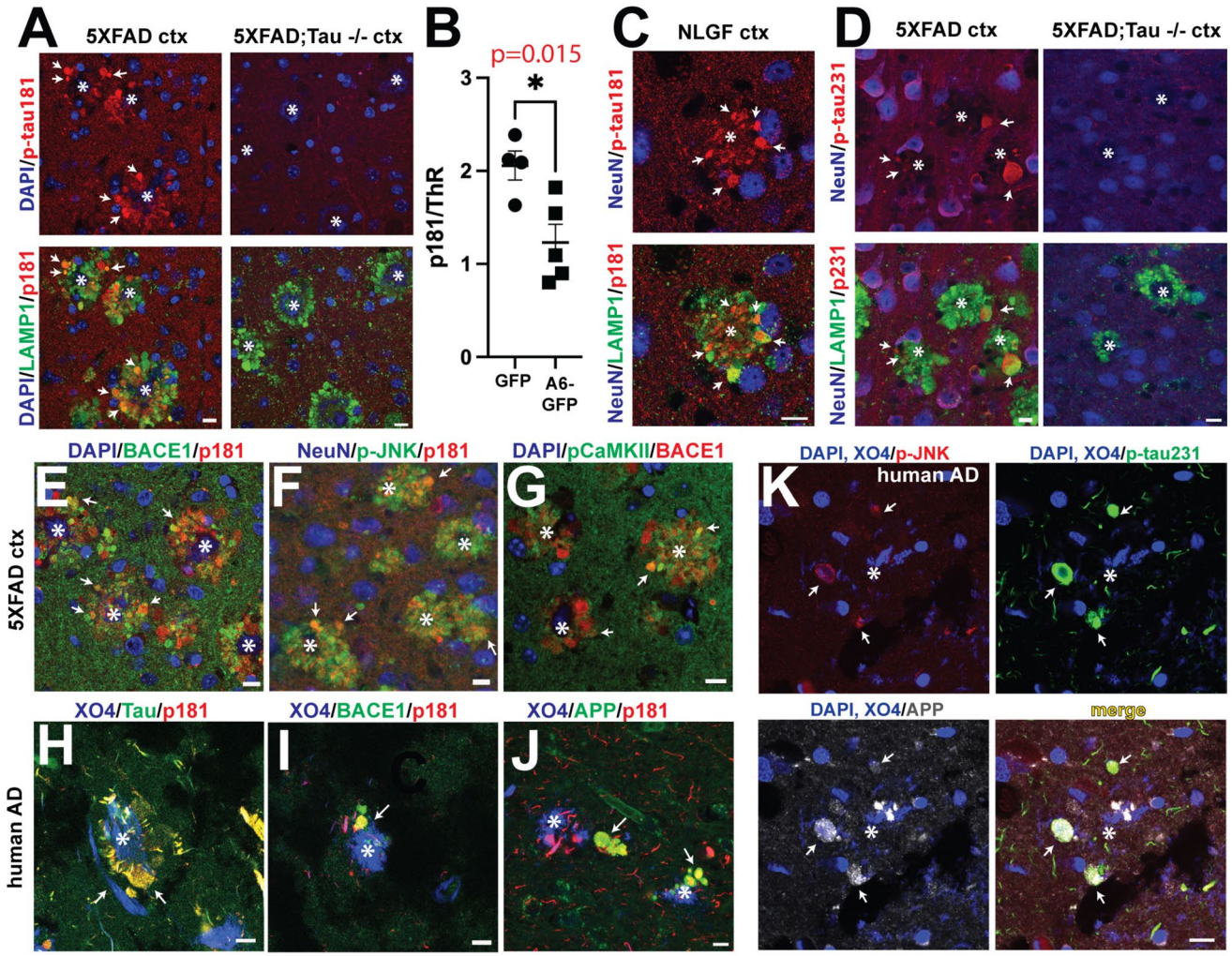

Fig. 6 p-tau181, p-tau231, and phosphorylated tau kinases increase in 5XFAD, APP-NLGF, and human AD dystrophic neurites, while annexin A6-GFP expression decreases p-tau181. **A** 5XFAD (left) and 5XFAD;Tau$^{-/-}$ (right) cortex (ctx) sections immunostained for p-tau181 (red), LAMP1 (green), and DAPI (blue). In 5XFAD brain, p-tau181 accumulates in LAMP1+ DNs in contact with amyloid plaques. Note that 5XFAD;Tau$^{-/-}$ brain forms amyloid plaques and LAMP1+ DNs, but that 5XFAD;Tau$^{-/-}$ DNs lack p-tau181 accumulation. **B** p-tau181:Thiazine red (ThR; amyloid stain) ratio in 5XFAD mice transduced with AAV expressing GFP or A6-GFP driven by the neuron-specific synapsin promoter. Note that p-tau181:ThR ratio is significantly decreased in 5XFAD mice expressing A6-GFP. **C** APP-NLGF cortex section immunostained for p-tau181 (red), LAMP1 (green), and NeuN (blue). The accumulation of p-tau181 in DNs of APP-NLGF appears very similar to that of 5XFAD mice. **D** 5XFAD (left) and 5XFAD;Tau$^{-/-}$ (right) cortex sections immunostained for p-tau231 (red), LAMP1 (green), and NeuN (blue). **E–G** 5XFAD cortex sections immunostained for p-tau181 (red), p-JNK (green), p-CaMKII (green), BACE1 (red), NeuN (blue), and DAPI (blue). **H–J** AD hippocampal sections immunostained for p-tau181 (red), total tau (Tau5, green), MeX04 (amyloid stain, blue), BACE1 (green), and APP (green). **K** AD hippocampal section immunostained for *p*-tau231 (green), p-JNK (red), APP (gray), MeX04 (blue), and DAPI (blue). *, plaque cores; arrows, DNs. Bars=10 µm. Images representative from $n = 3$ mice

results strongly support the hypothesis that amyloid deposition leads to aberrant tau phosphorylation via the formation of DNs.

Since annexin A6-GFP overexpression reduced DNs in 5XFAD brain (Fig. 5), we hypothesized that A6-GFP would also decrease phosphorylated tau associated with DNs. Indeed, we observed a significant reduction in the ratio of p-tau181 to amyloid in 5XFAD mice injected with syn-A6-GFP AAV compared to those injected with syn-GFP AAV (Fig. 6B). We hypothesized that increased kinase activity in DNs could be responsible for p-tau accumulation. Activated, phosphorylated forms of two kinases, CaMKII and JNK, known to phosphorylate p-tau181, p-tau217, and p-tau231 [78, 117], colocalized with p-tau181 in 5XFAD DNs (Fig. 6E–G). In human AD brain, p-tau181 colocalized with total tau, BACE1, and APP in DNs around plaques (Fig. 6H–J) and p-tau 231 colocalized with p-JNK and the DN marker APP (Fig. 6K). Co-occurrence of p-tau with

p-JNK and p-CaMKII in DNs does not demonstrate a physical interaction in these structures, but does suggest that DNs could be sites of early tau phosphorylation, especially p-tau181, which is used as an early CSF and plasma biomarker that indicates amyloid pathology and predicts AD [19, 65, 107].

Reduced annexin A6 function results in more dystrophic neurites and increased p-tau181

To determine the effects of reduced annexin A6 function on DNs, we utilized a naturally occurring annexin A6 truncation (p.N32*) generated by altered splicing that introduces a premature stop codon, which results in a protein lacking the last four of the eight annexin repeats [108]. Even at low levels, A6 N32 protein exerts strong dominant-negative effects, blocking the assembly of the repair cap by preventing the recruitment of full-length annexin A6 and other repair cap components to the site of membrane damage [31, 108]. Using the P0 intracerebroventricular injections of AAV8 described previously, we overexpressed an N32 A6-GFP fusion protein in neurons of 5XFAD mice and found a loss of membrane localization compared to A6-GFP (Fig. 7A), which was also observed in non-transgenic mice (Suppl. Fig. 7). The average LAMP1:Aβ42 ratio was significantly increased in mice overexpressing N32 A6-GFP compared to those expressing A6-GFP (Fig. 7B). Additionally, the ratio of p-tau181 to amyloid as measured by MeX04 staining was significantly elevated by N32 A6-GFP (Fig. 7C). Together, the increase and decrease of DNs and p-tau181 caused by expression of N32 A6-GFP and A6-GFP, respectively, strongly suggest an important role for annexin A6 in the repair of Aβ-induced membrane damage and DN formation.

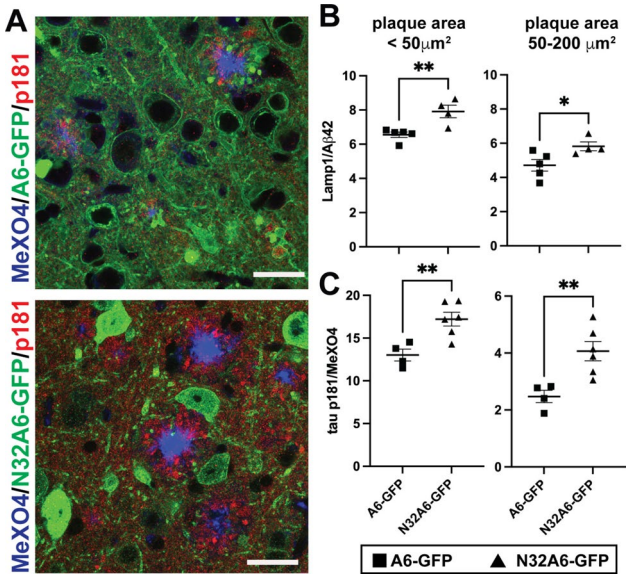

Fig. 7 Dominant negative annexin N32 A6-GFP increases dystrophic neurites and p-tau181 in 5XFAD brain. **A** Cortical sections of 5XFAD mice transduced with AAV expressing annexin A6-GFP or dominant-negative A6 truncation, N32 A6-GFP driven by the neuron-specific synapsin promoter immunostained for GFP (green), p-tau181 (red), and MeX04 (amyloid stain, blue). Note the mislocalization of N32 A6-GFP away from the plasma membrane toward the cytoplasm and nucleus in N32 A6-GFP compared to A6-GFP expressing neurons. Bar=25 μm. **B** LAMP1:Aβ42 ratio of amyloid plaques in the cortices of A6-GFP and N32 A6-GFP expressing 5XFAD mice binned by plaque core area with the indicated ranges in μm^2. Smaller, faster growing plaques in the size ranges < 50 μm^2 (left) and 50–200 μm^2 (right) of N32 A6-GFP expressing mice had significantly increased LAMP1:Aβ42 ratio compared to that of A6-GFP expressing mice. **C** The p-tau181:MeX04 ratio of amyloid plaques in the cortices of A6-GFP and N32 A6-GFP expressing 5XFAD mice binned by plaque core area with the indicated ranges in μm^2 (<50 μm^2, left; 50–200 μm^2, right). As with LAMP1/Aβ42 ratio (**B**), p-tau181:MeX04 ratio was significantly increased in smaller, faster growing plaques of N32 A6-GFP compared to A6-GFP expressing mice. $^{**}p < 0.01$, $^{*}p < 0.05$. $n = 4$–6 mice

Extracellular recombinant annexin A6-GFP localizes to membranes of dystrophic neurites

Previous work in skeletal muscle demonstrates that both intracellular annexin A6 overexpression and extracellular rA6 can enhance membrane repair [30]. Intracellular and extracellular annexin A6 promote myofiber membrane resealing after laser injury and reduce dye influx to equivalent amounts. Additionally, rA6 is also effective in acute (lytic damage from cardiotoxin injection) and chronic (muscular dystrophy due to sarcoglycan mutation) muscle injury models [30]. These results strongly suggest that rA6 could be an effective therapeutic agent, since it can home to sites of membrane damage from the extracellular space allowing exogenous administration of rA6. We previously published that exogenous rA6 localized to sites of laser damage on primary neurons [29], but we wanted to test whether extracellular rA6 would home to DNs *in vivo*. To do so, we administered a single stereotaxic injection of recombinant A6-HIS (Fig. 8A, B) or A6-GFP (Fig. 8C, D) into the lateral ventricle of 5XFAD (Fig. 8A,C, E) or APP-NLGF (Fig. 8B, D) mice and harvested brains 3 hours later. In the immediate vicinity of the needle track (Fig. 8E), A6-HIS strongly bound to damaged membranes resulting from the injection. Further from the injection site away from needle injury (boxed regions in Fig. 8E), immunofluorescence confocal microscopy revealed that both extracellular A6-HIS and A6-GFP localized to plasma membranes of BACE1- and LAMP1-positive DNs (Fig. 8A, B). In some cases (top panel Fig. 8A), rA6 completely coated the DN membrane, suggesting extensive externalization of phosphatidylserine, which could target the DN for engulfment and clearance by microglia or indicate cell death [101]. However, in most cases, we observed rA6 puncta more indicative of localized regions of membrane disruption. Although single stereotaxic

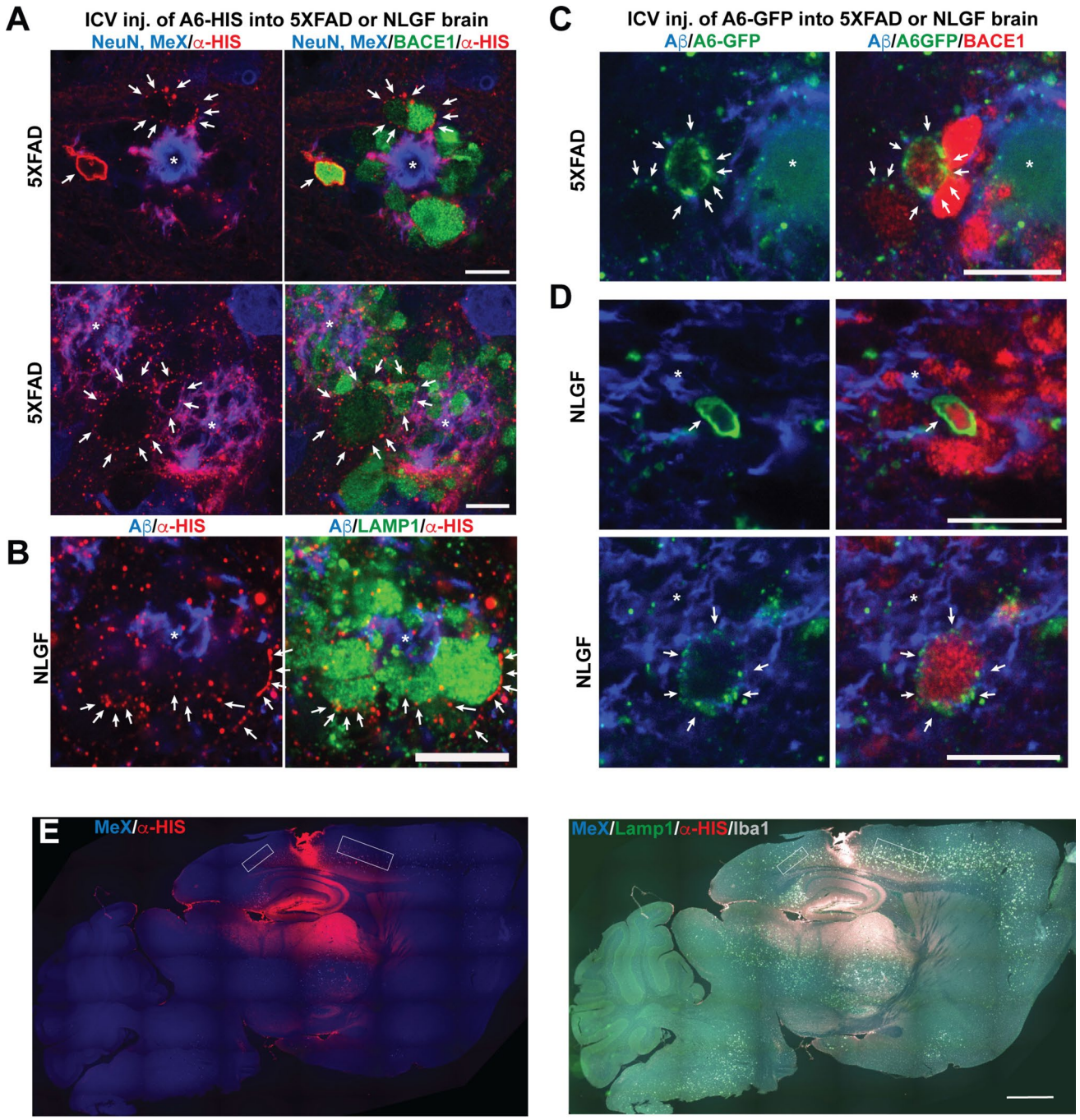

Fig. 8 Recombinant annexin A6 localizes to dystrophic neurites following intracerebral ventricular injection in 5XFAD and APP-NLGF mice. **A-D** Cortical sections from 5XFAD (**A**) and APP-NLGF (**B**) mice that received a single intracerebral ventricular (ICV) injection of recombinant annexin A6-HIS (3.3 mg/kg) or A6-GFP (0.9 mg/kg; **C** 5XFAD; **D** NLGF) and brains harvested 3 h later. Sections were immunostained for α-HIS (red), NeuN (blue), MeX04 (amyloid stain, blue), BACE1 (red), LAMP1 (green), and Aβ (3D6, blue). GFP fluorescence of A6-GFP was imaged in (**C**) and (**D**). Both recombinant A6-HIS and A6-GFP localized to membrane puncta and whole membranes on BACE1+ and LAMP1+ dystrophic neurites (arrows) in 5XFAD and APP-NLGF mice, indicating the presence of membrane damage. *, plaque cores; Bars=10μm. Representative from *n* = 2–5 mice per genotype, and protein injection. **E** Low magnification images of brain section from 5XFAD mouse after intracerebral ventricular (ICV) injection of recombinant annexin A6-HIS (3.3 mg/kg), immunostained with MethoxyX04 (blue) for amyloid, α-HIS (red), LAMP1 (green), and Iba1 (white) to demonstrate the spread of A6-HIS after three hours. White boxes indicate approximate areas at edge of injection spread selected for 60x confocal imaging in similar sections for A through D. Scale bar = 1000 μm

injections of rA6 are unlikely to have long-term therapeutic effects, they demonstrate that extracellular rA6 can in principle target damaged membranes on dystrophic neurites near amyloid plaques as a proof of concept for an AD therapy. Together, our results support further investigation of extracellular administration of rA6 as a potential novel therapeutic approach to limit Aβ-induced membrane damage for the prevention of dystrophic neurites in AD, which could have beneficial effects on tau pathology.

Discussion

In this work, we have demonstrated a role of annexin A6 in reducing DNs in the 5XFAD amyloid mouse model. We show that endogenous annexin A6 is found at the plasma membrane in neurons of mice and humans. In AD patients or AD mouse models, A6 localizes to the membrane of DNs in contact with amyloid plaques. Overexpression of wild-type annexin A6-GFP decreased DNs and p-tau181, while expression of dominant-negative truncated N32 A6-GFP increased DNs and p-tau181. We also demonstrate elevated calcium levels and calpain activity in DNs of 5XFAD mice. Additionally, we observed the presence of phosphorylated, active forms of tau kinases, such as p-CaMKII and p-JNK in DNs, which in combination with active calpain could lead to increased phosphorylation and cleavage of tau that promote aggregation-prone tau and tau seeding and spreading. Finally, we demonstrate that, as in other systems (muscle, heart, and primary neurons), exogenous recombinant annexin A6 can localize to and bind damaged neuronal membranes from the extracellular space, opening the possibility for a protein-based AD therapy.

The calcium hypothesis of AD posits that dysregulation of calcium homeostasis is the point of convergence of the many risk factors and molecular mechanisms that lead to development of AD and its associated neurodegeneration [3, 67]. Our work in this paper supports the calcium hypothesis, showing definitively that baseline resting calcium is elevated in DNs contacting Aβ plaques. Recent work demonstrates that DNs are detrimental, preventing effective transmission of action potentials and leading to loss of synaptic function [61, 120], which can contribute to cognitive decline. We further support the detrimental role of calcium influx in DNs by showing downstream changes, such as increased calpain activity, accumulation of phospho-tau epitopes, and phosphorylated forms of known tau kinases JNK and CaMKIIα, which is phosphorylated in the presence of high calcium [100].

As the "first responder" to calcium influx following membrane damage, annexin A6 plays the key role to initiate the formation of the membrane repair complex [30, 31]. Annexin A6 expression levels do not appear to be altered in the brains of either 5XFAD mice or AD patients (data not shown), but examples exist of recombinant and overexpressed annexins being used to protect against injury or damage in the brain. Previously, it was shown that recombinant annexin A6 or A5 reduced dye leakage from liposomes induced by Aβ and various membrane disruptors [23]. Injection of exogenous recombinant annexin A2 was protective in a traumatic brain injury model by decreasing blood–brain barrier (BBB) permeability and promoting angiogenesis [17], and annexin A5 protected choroid plexus cells from damage by Aβ42 [8]. Injection of human recombinant annexin A1 acutely decreased BBB permeability in young 5XFAD and Tau P301L mice, as well [95], further suggesting beneficial effects of annexins in neurological disease. Lentiviral overexpression of annexin A6 in mice improved outcomes after transient focal ischemia, minimizing loss of synaptic proteins [113]. Although annexin A6 constitutive null mice were shown to have normal immune and cardiac function [52], more recently, they were found to have increased sensitivity to painful mechanical stimuli due to loss of annexin A6 interaction with the Piezo2 channel [94]. These data support the idea that annexins A1, A2, A5, and A6 all play a role in protecting the brain.

In muscle, it is clear that annexins A1 and A2 work with annexin A6 in membrane repair, but in most neurons, little or no annexins A1 and A2 are expressed to interact with annexin A6 to form the membrane repair cap. Annexins A1 and A2 are expressed in the brain, but primarily in endothelial cells (Supplemental Fig. 4). It is known that annexins, such as A1 and A2, are found extracellularly, likely secreted through non-canonical pathways [93], and recent publications report that annexins A2 and A6 are found at high levels in the extracellular matrix of muscle where they promote myoblast motility [76]. Annexins A7 and A11 are highly expressed in the majority of neuronal cell types, like annexin A6, where they localize to plasma and nuclear membranes (A11) or to cytoplasm (A7), so it is possible they could interact with annexin A6 to facilitate membrane repair. Annexins A11 and A7 are unique in the annexin family in having a long unstructured N-terminus [44], which for annexin A11 is involved in RNA binding. Annexin A11 tethers mRNA to lysosomes for transport in neurons, and mutations disrupting this function are associated with amyotrophic lateral sclerosis in humans [75, 85]. Annexin A7 recruits the Endosomal Sorting Complex Required for Transport III (ESCRT III) complex to sites of membrane damage and facilitates repair through calcium-triggered protein interactions [105], so annexin A7 could complement the repair functions of annexin A6.

While membrane repair is a key function of annexin A6, it has been observed to play a role in other cellular processes, suggesting the possibility that annexin A6 may have pleiotropic effects in neurons. It has been reported that the

extreme N-terminus of tau can interact with annexins A2 and A6 core domains in calcium-dependent manner, and that the annexin A6–tau interaction affects tau microtubule binding and sorting into the axon [41, 42]. This latter notion is supported by the localization of annexin A6 to the axon initial segment (AIS), where it seems to promote axon branching [116]. Additionally, a recent study profiling the tau interactome in typical compared to rapidly progressing AD found increased levels of annexin A6 in the tau interactome of typical AD, suggesting that the annexin A6–tau interaction may protect against tau pathology, or that higher levels of annexin A6 improve membrane repair leading to slower AD progression [118]. Finally, two recent large genome-wide association studies (GWAS) have reported protective associations with AD in *TNIP1* within 50 kb of *ANXA6* [9, 114]. While the lead SNP was located in a different gene, the partial contribution of *ANXA6* to this signal cannot be completely ruled out.

In our work, it is possible that annexin A6–tau interactions may have played a role in decreasing tau phosphorylation in DNs. Alternatively, overexpression of annexin A6 during postnatal developmental may have affected axon outgrowth, although we did not observe any differences in the brains of mice expressing either A6-GFP or GFP alone. In hepatocytes, annexin A6 is associated with membranes of endosomes, multivesicular bodies, and autophagosomes, where it likely plays a role in remodeling membrane architecture and promoting vesicle fusions [35, 36]. Therefore, although our results strongly suggest the mechanism of annexin A6 in reducing DNs and tau phosphorylation involves repair of Aβ-induced membrane damage, it is possible other annexin A6 mechanisms may be at play.

Our study has several limitations. Since recombinant annexin A6 (rA6) added exogenously to cells or tissue can home to sites of membrane damage and mediate repair from outside the cell, rA6 may have potential as a novel biologic therapy for AD. However, several issues need to be resolved before exogenous rA6 administration can be considered a viable therapeutic strategy. First, while our experiments demonstrate that genetically overexpressed annexin A6 from birth can reduce DNs and phosphorylated tau, it still must be shown that overexpression of annexin A6 at different stages of Aβ pathology can reduce the formation of DNs and phosphorylated tau. Additionally, although injected rA6 showed localization to the DN membranes, it is necessary to perform chronic administration to determine whether rA6 can protect against DNs and tau phosphorylation. Current work is focused on the effects of AAV-mediated annexin A6 overexpression in adult mice that have Aβ pathology, chronic rA6 delivery through osmotic mini-pumps, and development of methods for delivery of rA6 across the blood–brain barrier [115] to allow chronic peripheral administration of rA6 as a more clinically practical method of testing therapeutic applicability. Future work will also focus on testing the ability of overexpressed and exogenous annexin A6 to decrease DNs and prevent in amyloid mouse models the seeding and spreading of pathologic tau isolated from human AD brain. Further understanding of the role of Aβ-induced membrane damage in DN formation and how to prevent it promises to shed light on the pathologic linkage between Aβ and tau, one of the most profound mysteries of AD.

Supplementary Information The online version contains supplementary material available at https://doi.org/10.1007/s00401-025-02888-1.

Acknowledgements This work is funded by NIA RF1 AG081649 to RV and KRS, Cure Alzheimer's Fund Tau Consortium grant to RV and KRS, Ryan Family Foundation Research Acceleration Award to RV and KRS, NIH training grant 5T32HL007909-25 to EAW, DKPK, NIH 5R25GM121231-07 to KPG, NIH R01 NS047726 to EMM and ARD, with support from Lakeside Discovery. AJP, JG, and SM received support from Northwestern Summer Undergraduate Research Grants. Imaging work was performed at the Northwestern University Center for Advanced Microscopy (RRID: SCR_020996) generously supported by NCI CCSG P30 CA060553 awarded to the Robert H Lurie Comprehensive Cancer Center. Multiphoton microscopy was performed on a Nikon A1R multiphoton microscope, acquired through the support of NIH 1S10OD010398-01. Human hippocampal tissue was provided by the Mesulam Center for Cognitive Neurology and Alzheimer's Disease at Northwestern University (NIA P30 AG072977).

Author contributions Conceptualized and designed research: KRS, ARD, EMM, and RV. Performed experiments: KRS, KPG, AEE, AJP, MLL, AWK, JG, SM, EAW, DKPK, and JP. Analyzed data: KRS. Wrote draft: KRS. Edited final manuscript: KRS, DP, BB, SJL, ARD, EMM, and RV. Analysis of human mutations: DP, RET, BB, and SJL. All authors viewed and approved manuscript.

Funding This work was funded by National Institutes of Health, under Grant Nos. RF1 AG081649, 5R25GM121231-07, 5T32HL007909-25, 5T32HL007909-25, RF1 AG081649, RF1 AG081649, and RF1 AG081649, Cure Alzheimer's Fund, Ryan Family Foundation Research Acceleration Award, Northwestern Undergraduate Research Fellowship, and Lakeside Discovery.

Declarations

Conflict of interest Northwestern University filed a US provisional patent application on behalf of KRS, ARD, EMM, and RV related to the use of annexins in treating neuronal cell membrane injury in September 2022.

References

1. (2023) The Alzheimer's Association, Alzheimer's Disease: Facts and Figures https://www.alz.org/alzheimers-dementia/facts-figures
2. Alexander GC, Emerson S, Kesselheim AS (2021) Evaluation of aducanumab for alzheimer disease: scientific evidence and regulatory review involving efficacy, safety, and futility. JAMA 325:1717–1718. https://doi.org/10.1001/jama.2021.3854
3. Alzheimer's Association Calcium Hypothesis W (2017) Calcium hypothesis of Alzheimer's disease and brain aging: a framework for integrating new evidence into a comprehensive theory of pathogenesis. Alzheimers Dement 13(178–182):e117. https://doi.org/10.1016/j.jalz.2016.12.006
4. Arai H, Lee VM, Otvos L Jr, Greenberg BD, Lowery DE, Sharma SK et al (1990) Defined neurofilament, tau, and beta-amyloid precursor protein epitopes distinguish Alzheimer from non-Alzheimer senile plaques. Proc Natl Acad Sci U S A 87:2249–2253. https://doi.org/10.1073/pnas.87.6.2249
5. Aschenbrenner AJ, Gordon BA, Benzinger TLS, Morris JC, Hassenstab JJ (2018) Influence of tau PET, amyloid PET, and hippocampal volume on cognition in Alzheimer disease. Neurology 91:e859–e866. https://doi.org/10.1212/WNL.0000000000006075
6. Barthelemy NR, Horie K, Sato C, Bateman RJ (2020) Blood plasma phosphorylated-tau isoforms track CNS change in Alzheimer's disease. J Exp Med. https://doi.org/10.1084/jem.20200861
7. Barthelemy NR, Li Y, Joseph-Mathurin N, Gordon BA, Hassenstab J, Benzinger TLS et al (2020) A soluble phosphorylated tau signature links tau, amyloid and the evolution of stages of dominantly inherited Alzheimer's disease. Nat Med 26:398–407. https://doi.org/10.1038/s41591-020-0781-z
8. Bartolome F, Krzyzanowska A, de la Cueva M, Pascual C, Antequera D, Spuch C et al (2020) Annexin A5 prevents amyloid-beta-induced toxicity in choroid plexus: implication for Alzheimer's disease. Sci Rep 10:9391. https://doi.org/10.1038/s41598-020-66177-5
9. Bellenguez C, Kucukali F, Jansen IE, Kleineidam L, Moreno-Grau S, Amin N et al (2022) New insights into the genetic etiology of Alzheimer's disease and related dementias. Nat Genet 54:412–436. https://doi.org/10.1038/s41588-022-01024-z
10. Boche D, Nicoll JAR (2020) Invited Review - Understanding cause and effect in Alzheimer's pathophysiology: implications for clinical trials. Neuropathol Appl Neurobiol 46:623–640. https://doi.org/10.1111/nan.12642
11. Boyarko B, Hook V (2021) Human Tau isoforms and proteolysis for production of toxic tau fragments in neurodegeneration. Front Neurosci 15:702788. https://doi.org/10.3389/fnins.2021.702788
12. Braun A, Pinyol R, Dahlhaus R, Koch D, Fonarev P, Grant BD et al (2005) EHD proteins associate with syndapin I and II and such interactions play a crucial role in endosomal recycling. Mol Biol Cell 16:3642–3658. https://doi.org/10.1091/mbc.e05-01-0076
13. Buggia-Prevot V, Fernandez CG, Udayar V, Vetrivel KS, Elie A, Roseman J et al (2013) A function for EHD family proteins in unidirectional retrograde dendritic transport of BACE1 and Alzheimer's disease Abeta production. Cell Rep 5:1552–1563. https://doi.org/10.1016/j.celrep.2013.12.006
14. Chan KY, Jang MJ, Yoo BB, Greenbaum A, Ravi N, Wu WL et al (2017) Engineered AAVs for efficient noninvasive gene delivery to the central and peripheral nervous systems. Nat Neurosci 20:1172–1179. https://doi.org/10.1038/nn.4593
15. Chen G, McKay NS, Gordon BA, Liu J, Joseph-Mathurin N, Schindler SE et al (2024) Predicting cognitive decline: Which is more useful, baseline amyloid levels or longitudinal change? Neuroimage Clin 41:103551. https://doi.org/10.1016/j.nicl.2023.103551
16. Chen TW, Wardill TJ, Sun Y, Pulver SR, Renninger SL, Baohan A et al (2013) Ultrasensitive fluorescent proteins for imaging neuronal activity. Nature 499:295–300. https://doi.org/10.1038/nature12354
17. Cheng C, Wang X, Jiang Y, Li Y, Liao Z, Li W et al (2021) Recombinant annexin A2 administration improves neurological outcomes after traumatic brain injury in mice. Front Pharmacol 12:708469. https://doi.org/10.3389/fphar.2021.708469
18. Cho H, Choi JY, Lee HS, Lee JH, Ryu YH, Lee MS et al (2019) Progressive tau accumulation in alzheimer disease: 2-year follow-up study. J Nucl Med 60:1611–1621. https://doi.org/10.2967/jnumed.118.221697
19. Clark C, Lewczuk P, Kornhuber J, Richiardi J, Marechal B, Karikari TK et al (2021) Plasma neurofilament light and phosphorylated tau 181 as biomarkers of Alzheimer's disease pathology and clinical disease progression. Alzheimers Res Ther 13:65. https://doi.org/10.1186/s13195-021-00805-8
20. Condello C, Schain A, Grutzendler J (2011) Multicolor timestamp reveals the dynamics and toxicity of amyloid deposition. Sci Rep 1:19. https://doi.org/10.1038/srep00019
21. Condello C, Yuan P, Schain A, Grutzendler J (2015) Microglia constitute a barrier that prevents neurotoxic protofibrillar Abeta42 hotspots around plaques. Nat Commun 6:6176. https://doi.org/10.1038/ncomms7176
22. Cras P, Kawai M, Lowery D, Gonzalez-DeWhitt P, Greenberg B, Perry G (1991) Senile plaque neurites in Alzheimer disease accumulate amyloid precursor protein. Proc Natl Acad Sci U S A 88:7552–7556. https://doi.org/10.1073/pnas.88.17.7552
23. Creutz CE, Hira JK, Gee VE, Eaton JM (2012) Protection of the membrane permeability barrier by annexins. Biochemistry 51:9966–9983. https://doi.org/10.1021/bi3013559
24. Cummings BJ, Su JH, Geddes JW, Van Nostrand WE, Wagner SL, Cunningham DD et al (1992) Aggregation of the amyloid precursor protein within degenerating neurons and dystrophic neurites in Alzheimer's disease. Neuroscience 48:763–777. https://doi.org/10.1016/0306-4522(92)90265-4
25. Dawson HN, Ferreira A, Eyster MV, Ghoshal N, Binder LI, Vitek MP (2001) Inhibition of neuronal maturation in primary hippocampal neurons from tau deficient mice. J Cell Sci 114:1179–1187. https://doi.org/10.1242/jcs.114.6.1179
26. De Rossi P, Andrew RJ, Musial TF, Buggia-Prevot V, Xu G, Ponnusamy M et al (2019) Aberrant accrual of BIN1 near Alzheimer's disease amyloid deposits in transgenic models. Brain Pathol 29:485–501. https://doi.org/10.1111/bpa.12687
27. De Rossi P, Buggia-Prevot V, Clayton BL, Vasquez JB, van Sanford C, Andrew RJ et al (2016) Predominant expression of Alzheimer's disease-associated BIN1 in mature oligodendrocytes and localization to white matter tracts. Mol Neurodegener 11:59. https://doi.org/10.1186/s13024-016-0124-1
28. Demonbreun AR, Allen MV, Warner JL, Barefield DY, Krishnan S, Swanson KE et al (2016) Enhanced muscular dystrophy from loss of dysferlin is accompanied by impaired annexin A6 translocation after sarcolemmal disruption. Am J Pathol 186:1610–1622. https://doi.org/10.1016/j.ajpath.2016.02.005
29. Demonbreun AR, Bogdanovic E, Vaught LA, Reiser NL, Fallon KS, Long AM et al (2022) A conserved annexin A6-mediated membrane repair mechanism in muscle, heart, and nerve. JCI Insight. https://doi.org/10.1172/jci.insight.158107
30. Demonbreun AR, Fallon KS, Oosterbaan CC, Bogdanovic E, Warner JL, Sell JJ et al (2019) Recombinant annexin A6 promotes membrane repair and protects against muscle injury. J Clin Invest 129:4657–4670. https://doi.org/10.1172/JCI128840

31. Demonbreun AR, Quattrocelli M, Barefield DY, Allen MV, Swanson KE, McNally EM (2016) An actin-dependent annexin complex mediates plasma membrane repair in muscle. J Cell Biol 213:705–718. https://doi.org/10.1083/jcb.201512022
32. DeTure MA, Dickson DW (2019) The neuropathological diagnosis of Alzheimer's disease. Mol Neurodegener 14:32. https://doi.org/10.1186/s13024-019-0333-5
33. Drolle E, Negoda A, Hammond K, Pavlov E, Leonenko Z (2017) Changes in lipid membranes may trigger amyloid toxicity in Alzheimer's disease. PLoS ONE 12:e0182194. https://doi.org/10.1371/journal.pone.0182194
34. Eberhard DA, Brown MD, VandenBerg SR (1994) Alterations of annexin expression in pathological neuronal and glial reactions. Immunohistochemical localization of annexins I, II (p36 and p11 subunits), IV, and VI in the human hippocampus. Am J Pathol 145:640–649
35. Enrich C, Rentero C, de Muga SV, Reverter M, Mulay V, Wood P et al (2011) Annexin A6-Linking Ca(2+) signaling with cholesterol transport. Biochim Biophys Acta 1813:935–947. https://doi.org/10.1016/j.bbamcr.2010.09.015
36. Enrich C, Rentero C, Grewal T (2017) Annexin A6 in the liver: From the endocytic compartment to cellular physiology. Biochim Biophys Acta Mol Cell Res 1864:933–946. https://doi.org/10.1016/j.bbamcr.2016.10.017
37. Fernandez-Perez EJ, Peters C, Aguayo LG (2016) Membrane damage induced by amyloid beta and a potential link with neuroinflammation. Curr Pharm Des 22:1295–1304. https://doi.org/10.2174/1381612822101603041117 02
38. Ferreira A, Bigio EH (2011) Calpain-mediated tau cleavage: a mechanism leading to neurodegeneration shared by multiple tauopathies. Mol Med 17:676–685. https://doi.org/10.2119/molmed.2010.00220
39. Galvin JE, Palamand D, Strider J, Milone M, Pestronk A (2006) The muscle protein dysferlin accumulates in the Alzheimer brain. Acta Neuropathol 112:665–671. https://doi.org/10.1007/s00401-006-0147-8
40. Gao P, Ye L, Cheng H, Li H (2021) The mechanistic role of bridging integrator 1 (BIN1) in Alzheimer's disease. Cell Mol Neurobiol 41:1431–1440. https://doi.org/10.1007/s10571-020-00926-y
41. Gauthier-Kemper A, Suarez Alonso M, Sundermann F, Niewidok B, Fernandez MP, Bakota L et al (2018) Annexins A2 and A6 interact with the extreme N terminus of tau and thereby contribute to tau's axonal localization. J Biol Chem 293:8065–8076. https://doi.org/10.1074/jbc.RA117.000490
42. Gauthier-Kemper A, Weissmann C, Golovyashkina N, Sebo-Lemke Z, Drewes G, Gerke V et al (2011) The frontotemporal dementia mutation R406W blocks tau's interaction with the membrane in an annexin A2-dependent manner. J Cell Biol 192:647–661. https://doi.org/10.1083/jcb.201007161
43. George M, Ying G, Rainey MA, Solomon A, Parikh PT, Gao Q et al (2007) Shared as well as distinct roles of EHD proteins revealed by biochemical and functional comparisons in mammalian cells and C. elegans. BMC Cell Biol. https://doi.org/10.1186/1471-2121-8-3
44. Gerke V, Gavins FNE, Geisow M, Grewal T, Jaiswal JK, Nylandsted J et al (2024) Annexins-a family of proteins with distinctive tastes for cell signaling and membrane dynamics. Nat Commun 15:1574. https://doi.org/10.1038/s41467-024-45954-0
45. Gonzalez-Ortiz F, Kac PR, Brum WS, Zetterberg H, Blennow K, Karikari TK (2023) Plasma phospho-tau in Alzheimer's disease: towards diagnostic and therapeutic trial applications. Mol Neurodegener 18:18. https://doi.org/10.1186/s13024-023-00605-8
46. Gowrishankar S, Yuan P, Wu Y, Schrag M, Paradise S, Grutzendler J et al (2015) Massive accumulation of luminal protease-deficient axonal lysosomes at Alzheimer's disease amyloid plaques. Proc Natl Acad Sci U S A 112:E3699-3708. https://doi.org/10.1073/pnas.1510329112
47. Gratuze M, Chen Y, Parhizkar S, Jain N, Strickland MR, Serrano JR et al (2021) Activated microglia mitigate Abeta-associated tau seeding and spreading. J Exp Med. https://doi.org/10.1084/jem.20210542
48. Grewal T, Rentero C, Enrich C, Wahba M, Raabe CA, Rescher U (2021) Annexin animal models-from fundamental principles to translational research. Int J Mol Sci. https://doi.org/10.3390/ijms22073439
49. Hanseeuw BJ, Betensky RA, Jacobs HIL, Schultz AP, Sepulcre J, Becker JA et al (2019) Association of amyloid and tau with cognition in preclinical alzheimer disease: a longitudinal study. JAMA Neurol 76:915–924. https://doi.org/10.1001/jamaneurol.2019.1424
50. Hansson O (2021) Biomarkers for neurodegenerative diseases. Nat Med 27:954–963. https://doi.org/10.1038/s41591-021-01382-x
51. Hardy J (2017) Membrane damage is at the core of Alzheimer's disease. Lancet Neurol 16:342. https://doi.org/10.1016/S1474-4422(17)30091-1
52. Hawkins TE, Roes J, Rees D, Monkhouse J, Moss SE (1999) Immunological development and cardiovascular function are normal in annexin VI null mutant mice. Mol Cell Biol 19:8028–8032. https://doi.org/10.1128/MCB.19.12.8028
53. He Z, Guo JL, McBride JD, Narasimhan S, Kim H, Changolkar L et al (2018) Amyloid-beta plaques enhance Alzheimer's brain tau-seeded pathologies by facilitating neuritic plaque tau aggregation. Nat Med 24:29–38. https://doi.org/10.1038/nm.4443
54. Ho M, Post CM, Donahue LR, Lidov HG, Bronson RT, Goolsby H et al (2004) Disruption of muscle membrane and phenotype divergence in two novel mouse models of dysferlin deficiency. Hum Mol Genet 13:1999–2010. https://doi.org/10.1093/hmg/ddh212
55. Huang Q, Chan KY, Tobey IG, Chan YA, Poterba T, Boutros CL et al (2019) Delivering genes across the blood-brain barrier: LY6A, a novel cellular receptor for AAV-PHPB capsids. PLoS ONE 14:e0225206. https://doi.org/10.1371/journal.pone.0225206
56. Huang Y, Happonen KE, Burrola PG, O'Connor C, Hah N, Huang L et al (2021) Microglia use TAM receptors to detect and engulf amyloid beta plaques. Nat Immunol 22:586–594. https://doi.org/10.1038/s41590-021-00913-5
57. Jack CR Jr, Knopman DS, Jagust WJ, Shaw LM, Aisen PS, Weiner MW et al (2010) Hypothetical model of dynamic biomarkers of the Alzheimer's pathological cascade. Lancet Neurol 9:119–128. https://doi.org/10.1016/S1474-4422(09)70299-6
58. Jack CR Jr, Wiste HJ, Schwarz CG, Lowe VJ, Senjem ML, Vemuri P et al (2018) Longitudinal tau PET in ageing and Alzheimer's disease. Brain 141:1517–1528. https://doi.org/10.1093/brain/awy059
59. Jagust W (2018) Imaging the evolution and pathophysiology of Alzheimer disease. Nat Rev Neurosci 19:687–700. https://doi.org/10.1038/s41583-018-0067-3
60. Janelidze S, Bali D, Ashton NJ, Barthelemy NR, Vanbrabant J, Stoops E et al (2023) Head-to-head comparison of 10 plasma phospho-tau assays in prodromal Alzheimer's disease. Brain 146:1592–1601. https://doi.org/10.1093/brain/awac333
61. Jang J, Yeo S, Baek S, Jung HJ, Lee MS, Choi SH et al (2023) Abnormal accumulation of extracellular vesicles in hippocampal dystrophic axons and regulation by the primary cilia in Alzheimer's disease. Acta Neuropathol Commun 11:142. https://doi.org/10.1186/s40478-023-01637-3
62. Jorda-Siquier T, Petrel M, Kouskoff V, Smailovic U, Cordelieres F, Frykman S et al (2022) APP accumulates with presynaptic

proteins around amyloid plaques: a role for presynaptic mechanisms in Alzheimer's disease? Alzheimers Dement 18:2099–2116. https://doi.org/10.1002/alz.12546
63. Jury-Garfe N, Redding-Ochoa J, You Y, Martinez P, Karahan H, Chimal-Juarez E et al (2024) Enhanced microglial dynamics and a paucity of tau seeding in the amyloid plaque microenvironment contribute to cognitive resilience in Alzheimer's disease. Acta Neuropathol 148:15. https://doi.org/10.1007/s00401-024-02775-1
64. Kandalepas PC, Sadleir KR, Eimer WA, Zhao J, Nicholson DA, Vassar R (2013) The Alzheimer's beta-secretase BACE1 localizes to normal presynaptic terminals and to dystrophic presynaptic terminals surrounding amyloid plaques. Acta Neuropathol 126:329–352. https://doi.org/10.1007/s00401-013-1152-3
65. Karikari TK, Emersic A, Vrillon A, Lantero-Rodriguez J, Ashton NJ, Kramberger MG et al (2021) Head-to-head comparison of clinical performance of CSF phospho-tau T181 and T217 biomarkers for Alzheimer's disease diagnosis. Alzheimers Dement 17:755–767. https://doi.org/10.1002/alz.12236
66. Karran E, De Strooper B (2022) The amyloid hypothesis in Alzheimer disease: new insights from new therapeutics. Nat Rev Drug Discov 21:306–318. https://doi.org/10.1038/s41573-022-00391-w
67. Khachaturian ZS (1984) Towards theories of brain aging. In: Kay DS (ed) Handbook of studies on psychiatry and old age. Elsevier Science Publishers, B. V., City, pp 7–30
68. Kuchibhotla KV, Goldman ST, Lattarulo CR, Wu HY, Hyman BT, Bacskai BJ (2008) Abeta plaques lead to aberrant regulation of calcium homeostasis in vivo resulting in structural and functional disruption of neuronal networks. Neuron 59:214–225. https://doi.org/10.1016/j.neuron.2008.06.008
69. La Joie R, Visani AV, Baker SL, Brown JA, Bourakova V, Cha J et al (2020) Prospective longitudinal atrophy in Alzheimer's disease correlates with the intensity and topography of baseline tau-PET. Sci Transl Med. https://doi.org/10.1126/scitranslmed.aau5732
70. Lambert JC, Zelenika D, Hiltunen M, Chouraki V, Combarros O, Bullido MJ et al (2011) Evidence of the association of BIN1 and PICALM with the AD risk in contrasting European populations. Neurobiol Aging 32(756):e711-755. https://doi.org/10.1016/j.neurobiolaging.2010.11.022
71. Levites Y, Jansen K, Smithson LA, Dakin R, Holloway VM, Das P et al (2006) Intracranial adeno-associated virus-mediated delivery of anti-pan amyloid beta, amyloid beta40, and amyloid beta42 single-chain variable fragments attenuates plaque pathology in amyloid precursor protein mice. J Neurosci 26:11923–11928. https://doi.org/10.1523/JNEUROSCI.2795-06.2006
72. Leyns CEG, Gratuze M, Narasimhan S, Jain N, Koscal LJ, Jiang H et al (2019) TREM2 function impedes tau seeding in neuritic plaques. Nat Neurosci 22:1217–1222. https://doi.org/10.1038/s41593-019-0433-0
73. Li T, Braunstein KE, Zhang J, Lau A, Sibener L, Deeble C et al (2016) The neuritic plaque facilitates pathological conversion of tau in an Alzheimer's disease mouse model. Nat Commun 7:12082. https://doi.org/10.1038/ncomms12082
74. Liang B, Duan BY, Zhou XP, Gong JX, Luo ZG (2010) Calpain activation promotes BACE1 expression, amyloid precursor protein processing, and amyloid plaque formation in a transgenic mouse model of Alzheimer disease. J Biol Chem 285:27737–27744. https://doi.org/10.1074/jbc.M110.117960
75. Liao YC, Fernandopulle MS, Wang G, Choi H, Hao L, Drerup CM et al (2019) RNA Granules Hitchhike on Lysosomes for Long-Distance Transport, Using Annexin A11 as a Molecular Tether. Cell 179(147–164):e120. https://doi.org/10.1016/j.cell.2019.08.050
76. Long AM, Kwon JM, Lee G, Reiser NL, Vaught LA, O'Brien JG et al (2024) The extracellular matrix differentially directs myoblast motility and differentiation in distinct forms of muscular dystrophy: dystrophic matrices alter myoblast motility. Matrix Biol 129:44–58. https://doi.org/10.1016/j.matbio.2024.04.001
77. Mabrouk R, Miettinen PO, Tanila H (2023) Most dystrophic neurites in the common 5xFAD Alzheimer mouse model originate from axon terminals. Neurobiol Dis 182:106150. https://doi.org/10.1016/j.nbd.2023.106150
78. Martin L, Latypova X, Wilson CM, Magnaudeix A, Perrin ML, Yardin C et al (2013) Tau protein kinases: involvement in Alzheimer's disease. Ageing Res Rev 12:289–309. https://doi.org/10.1016/j.arr.2012.06.003
79. Mattsson-Carlgren N, Andersson E, Janelidze S, Ossenkoppele R, Insel P, Strandberg O et al (2020) Abeta deposition is associated with increases in soluble and phosphorylated tau that precede a positive Tau PET in Alzheimer's disease. Sci Adv 6:eaaz2387. https://doi.org/10.1126/sciadv.aaz2387
80. Mattsson-Carlgren N, Leuzy A, Janelidze S, Palmqvist S, Stomrud E, Strandberg O et al (2020) The implications of different approaches to define AT(N) in Alzheimer disease. Neurology 94:e2233–e2244. https://doi.org/10.1212/WNL.0000000000009485
81. McCartney CE, MacLeod JA, Greer PA, Davies PL (2018) An easy-to-use FRET protein substrate to detect calpain cleavage in vitro and in vivo. Biochim Biophys Acta Mol Cell Res 1865:221–230. https://doi.org/10.1016/j.bbamcr.2017.10.013
82. Medeiros R, Kitazawa M, Chabrier MA, Cheng D, Baglietto-Vargas D, Kling A et al (2012) Calpain inhibitor A-705253 mitigates Alzheimer's disease-like pathology and cognitive decline in aged 3xTgAD mice. Am J Pathol 181:616–625. https://doi.org/10.1016/j.ajpath.2012.04.020
83. Mormino EC, Papp KV (2018) Amyloid accumulation and cognitive decline in clinically normal older individuals: implications for aging and early Alzheimer's disease. J Alzheimers Dis 64:S633–S646. https://doi.org/10.3233/JAD-179928
84. Mullard A (2024) FDA approves third anti-amyloid antibody for Alzheimer disease. Nat Rev Drug Discov 23:571. https://doi.org/10.1038/d41573-024-00116-1
85. Nahm M, Lim SM, Kim YE, Park J, Noh MY, Lee S et al (2020) ANXA11 mutations in ALS cause dysregulation of calcium homeostasis and stress granule dynamics. Sci Transl Med. https://doi.org/10.1126/scitranslmed.aax3993
86. Oakley H, Cole SL, Logan S, Maus E, Shao P, Craft J et al (2006) Intraneuronal beta-amyloid aggregates, neurodegeneration, and neuron loss in transgenic mice with five familial Alzheimer's disease mutations: potential factors in amyloid plaque formation. J Neurosci 26:10129–10140
87. Ossenkoppele R, Rabinovici GD, Smith R, Cho H, Scholl M, Strandberg O et al (2018) Discriminative accuracy of [18F]flortaucipir positron emission tomography for alzheimer disease vs other neurodegenerative disorders. JAMA 320:1151–1162. https://doi.org/10.1001/jama.2018.12917
88. Palmqvist S, Insel PS, Stomrud E, Janelidze S, Zetterberg H, Brix B et al (2019) Cerebrospinal fluid and plasma biomarker trajectories with increasing amyloid deposition in Alzheimer's disease. EMBO Mol Med 11:e11170. https://doi.org/10.15252/emmm.201911170
89. Parhizkar S, Arzberger T, Brendel M, Kleinberger G, Deussing M, Focke C et al (2019) Loss of TREM2 function increases amyloid seeding but reduces plaque-associated ApoE. Nat Neurosci 22:191–204. https://doi.org/10.1038/s41593-018-0296-9
90. Park JC, Baik SH, Han SH, Cho HJ, Choi H, Kim HJ et al (2017) Annexin A1 restores Abeta1-42 -induced blood-brain barrier disruption through the inhibition of RhoA-ROCK

signaling pathway. Aging Cell 16:149–161. https://doi.org/10.1111/acel.12530
91. Park SY, Ferreira A (2005) The generation of a 17 kDa neurotoxic fragment: an alternative mechanism by which tau mediates beta-amyloid-induced neurodegeneration. J Neurosci 25:5365–5375. https://doi.org/10.1523/JNEUROSCI.1125-05.2005
92. Peters F, Salihoglu H, Pratsch K, Herzog E, Pigoni M, Sgobio C et al (2019) Tau deletion reduces plaque-associated BACE1 accumulation and decelerates plaque formation in a mouse model of Alzheimer's disease. EMBO J 38:e102345. https://doi.org/10.15252/embj.2019102345
93. Popa SJ, Stewart SE, Moreau K (2018) Unconventional secretion of annexins and galectins. Semin Cell Dev Biol 83:42–50. https://doi.org/10.1016/j.semcdb.2018.02.022
94. Raouf R, Lolignier S, Sexton JE, Millet Q, Santana-Varela S, Biller A et al (2018) Inhibition of somatosensory mechanotransduction by annexin A6. Sci Signal. https://doi.org/10.1126/scisignal.aao2060
95. Ries M, Watts H, Mota BC, Lopez MY, Donat CK, Baxan N et al (2021) Annexin A1 restores cerebrovascular integrity concomitant with reduced amyloid-beta and tau pathology. Brain 144:1526–1541. https://doi.org/10.1093/brain/awab050
96. Roberson ED, Scearce-Levie K, Palop JJ, Yan F, Cheng IH, Wu T et al (2007) Reducing endogenous tau ameliorates amyloid beta-induced deficits in an Alzheimer's disease mouse model. Science 316:750–754. https://doi.org/10.1126/science.1141736
97. Robert A, Scholl M, Vogels T (2021) Tau seeding mouse models with patient brain-derived aggregates. Int J Mol Sci. https://doi.org/10.3390/ijms22116132
98. Sadleir KR, Kandalepas PC, Buggia-Prevot V, Nicholson DA, Thinakaran G, Vassar R (2016) Presynaptic dystrophic neurites surrounding amyloid plaques are sites of microtubule disruption, BACE1 elevation, and increased Abeta generation in Alzheimer's disease. Acta Neuropathol 132:235–256. https://doi.org/10.1007/s00401-016-1558-9
99. Sanchez-Ponce D, DeFelipe J, Garrido JJ, Munoz A (2011) In vitro maturation of the cisternal organelle in the hippocampal neuron's axon initial segment. Mol Cell Neurosci 48:104–116. https://doi.org/10.1016/j.mcn.2011.06.010
100. Schulman H, Greengard P (1978) Stimulation of brain membrane protein phosphorylation by calcium and an endogenous heat-stable protein. Nature 271:478–479. https://doi.org/10.1038/271478a0
101. Scott-Hewitt N, Perrucci F, Morini R, Erreni M, Mahoney M, Witkowska A et al (2020) Local externalization of phosphatidylserine mediates developmental synaptic pruning by microglia. EMBO J 39:e105380. https://doi.org/10.15252/embj.2020105380
102. Seshadri S, Fitzpatrick AL, Ikram MA, DeStefano AL, Gudnason V, Boada M et al (2010) Genome-wide analysis of genetic loci associated with Alzheimer disease. JAMA 303:1832–1840. https://doi.org/10.1001/jama.2010.574
103. Sinjoanu RC, Kleinschmidt S, Bitner RS, Brioni JD, Moeller A, Ferreira A (2008) The novel calpain inhibitor A-705253 potently inhibits oligomeric beta-amyloid-induced dynamin 1 and tau cleavage in hippocampal neurons. Neurochem Int 53:79–88. https://doi.org/10.1016/j.neuint.2008.06.003
104. Sivaramakrishnan S, Spudich JA (2011) Systematic control of protein interaction using a modular ER/K alpha-helix linker. Proc Natl Acad Sci U S A 108:20467–20472. https://doi.org/10.1073/pnas.1116066108
105. Sonder SL, Boye TL, Tolle R, Dengjel J, Maeda K, Jaattela M et al (2019) Annexin A7 is required for ESCRT III-mediated plasma membrane repair. Sci Rep 9:6726. https://doi.org/10.1038/s41598-019-43143-4
106. Su JH, Cummings BJ, Cotman CW (1993) Identification and distribution of axonal dystrophic neurites in Alzheimer's disease. Brain Res 625:228–237. https://doi.org/10.1016/0006-8993(93)91063-x
107. Suarez-Calvet M, Karikari TK, Ashton NJ, Lantero Rodriguez J, Mila-Aloma M, Gispert JD et al (2020) Novel tau biomarkers phosphorylated at T181, T217 or T231 rise in the initial stages of the preclinical Alzheimer's continuum when only subtle changes in Abeta pathology are detected. EMBO Mol Med 12:e12921. https://doi.org/10.15252/emmm.202012921
108. Swaggart KA, Demonbreun AR, Vo AH, Swanson KE, Kim EY, Fahrenbach JP et al (2014) Annexin A6 modifies muscular dystrophy by mediating sarcolemmal repair. Proc Natl Acad Sci U S A 111:6004–6009. https://doi.org/10.1073/pnas.1324242111
109. Swanson CJ, Sivaramakrishnan S (2014) Harnessing the unique structural properties of isolated alpha-helices. J Biol Chem 289:25460–25467. https://doi.org/10.1074/jbc.R114.583906
110. Tan MS, Yu JT, Tan L (2013) Bridging integrator 1 (BIN1): form, function, and Alzheimer's disease. Trends Mol Med 19:594–603. https://doi.org/10.1016/j.molmed.2013.06.004
111. Tsering W, Prokop S (2024) Neuritic Plaques - Gateways to Understanding Alzheimer's Disease. Mol Neurobiol 61:2808–2821. https://doi.org/10.1007/s12035-023-03736-7
112. Turner RS, Suzuki N, Chyung AS, Younkin SG, Lee VM (1996) Amyloids beta40 and beta42 are generated intracellularly in cultured human neurons and their secretion increases with maturation. J Biol Chem 271:8966–8970. https://doi.org/10.1074/jbc.271.15.8966
113. Wang Y, Yang Z, Wang R, Zheng Y, Han Z, Fan J et al (2024) Annexin A6 mitigates neurological deficit in ischemia/reperfusion injury by promoting synaptic plasticity. CNS Neurosci Ther 30:e14639. https://doi.org/10.1111/cns.14639
114. Wightman DP, Jansen IE, Savage JE, Shadrin AA, Bahrami S, Holland D et al (2021) A genome-wide association study with 1,126,563 individuals identifies new risk loci for Alzheimer's disease. Nat Genet 53:1276–1282. https://doi.org/10.1038/s41588-021-00921-z
115. Wu D, Chen Q, Chen X, Han F, Chen Z, Wang Y (2023) The blood-brain barrier: structure, regulation, and drug delivery. Signal Transduct Target Ther 8:217. https://doi.org/10.1038/s41392-023-01481-w
116. Yamatani H, Kawasaki T, Mita S, Inagaki N, Hirata T (2010) Proteomics analysis of the temporal changes in axonal proteins during maturation. Dev Neurobiol 70:523–537. https://doi.org/10.1002/dneu.20794
117. Yarza R, Vela S, Solas M, Ramirez MJ (2015) c-Jun N-terminal kinase (JNK) signaling as a therapeutic target for Alzheimer's Disease. Front Pharmacol 6:321. https://doi.org/10.3389/fphar.2015.00321
118. Younas N, Zafar S, Saleem T, Fernandez Flores LC, Younas A, Schmitz M et al (2023) Differential interactome mapping of aggregation prone/prion-like proteins under stress: novel links to stress granule biology. Cell Biosci 13:221. https://doi.org/10.1186/s13578-023-01164-7
119. Yuan P, Condello C, Keene CD, Wang Y, Bird TD, Paul SM et al (2016) TREM2 haplodeficiency in mice and humans impairs the microglia barrier function leading to decreased amyloid compaction and severe axonal dystrophy. Neuron 90:724–739. https://doi.org/10.1016/j.neuron.2016.05.003
120. Yuan P, Zhang M, Tong L, Morse TM, McDougal RA, Ding H et al (2022) PLD3 affects axonal spheroids and network defects in Alzheimer's disease. Nature 612:328–337. https://doi.org/10.1038/s41586-022-05491-6
121. Zhao J, Fu Y, Yasvoina M, Shao P, Hitt B, O'Connor T et al (2007) Beta-site amyloid precursor protein cleaving enzyme 1 levels become elevated in neurons around amyloid plaques: implications for Alzheimer's disease pathogenesis. J Neurosci 27:3639–3649

122. Zhao WQ, Lu B (2007) Expression of annexin A2 in GABAergic interneurons in the normal rat brain. J Neurochem 100:1211–1223. https://doi.org/10.1111/j.1471-4159.2006.04311.x